Postprint: Dastjerdi, Sh.; Tadi Beni, Y.; Malikan, M. A comprehensive study on nonlinear hygro-thermo-mechanical analysis of thick functionally graded porous rotating disk based on two quasi three-dimensional theories. MECHANICS BASED DESIGN OF STRUCTURES AND MACHINES, AN INTERNATIONAL JOURNAL, (2020).
https://doi.org/10.1080/15397734.2020.1814812

A comprehensive study on nonlinear hygro-thermo-mechanical analysis of thick functionally graded porous rotating disk based on two quasi three-dimensional theories

Shahriar Dastjerdi[a,b*], Yaghoub Tadi Beni[c], Mohammad Malikan[d]

[a]Department of Mechanical Engineering, Shahrood branch, Islamic Azad University, Shahrood, Iran

[b]Division of Mechanics, Civil Engineering Department, Akdeniz University, Antalya, Turkey

[c]Faculty of Engineering, Shahrekourd University, Shahrekord, Iran

[d]Department of Mechanics of Materials and Structures, Faculty of Civil and Environmental Engineering, Gdansk University of Technology, Gdansk, Poland

*Corresponding author: Tel: +98-9155055767

E-mail address: dastjerdi_shahriar@yahoo.com

ABSTRACT

In this paper, a highly efficient quasi three-dimensional theory has been used to study the nonlinear hygro-thermo-mechanical bending analysis of very thick functionally graded material (FGM) rotating disk in hygro-thermal environment considering the porosity as a structural defect. Two applied quasi three-dimensional displacement fields are assumed in which the strain along the thickness (ε_z) is not zero unlike most of the other plate theories. By considering the nonlinear strains (von Kármán's assumptions) the large deformations have also been taken into account in order to obtain more accurate results. Finally, some factors that affect the results have been studied further.

Keywords: Annular/circular FGM rotating disk; Quasi three-dimensional theory; Hygro-thermal environment; Porosity; Semi-Analytical Polynomial Method (SAPM)

1. Introduction

Functionally graded materials (FGMs) have been used widely because of their unique mechanical properties. The mechanical properties of FG materials are varied gradually into one or more directions. One of the most important application of FG materials relates to their especial thermal property. Because of the mentioned benefits of FG material, application of them can be observed remarkably. There are so many structures made of FG materials for improving their mechanical behaviors. One of the most important structures are plates that can be seen in various types of geometrical shapes. Analyses of functionally graded plates (FGPs) rely on plate theories**.** Generally, extensive studies related to FGPs are carried out by using the classical plate theory (CPT), first-order shear deformation plate theory (FSDT) and higher-order shear deformation theories (HSDTs). The FSDT considers a shear correction factor for supporting transverse shear effects, so it is appropriate for analysis of moderately thick and thin plates. In recent years, many shear deformation theories have been developed for the analysis of plates, beams and other structural elements. Shear deformation theories are categorized into two groups: the theories with thickness effect and the ones without thickness effect. One of HSDTs that the transverse displacement is expanded as a higher-order variation through the plate thickness is the quasi three-dimensional theory. There are several quasi-three-dimensional theories introduced in literature. In the following, various types of these references are listed.

The exact three-dimensional analysis gives the most accurate results in the analysis of mechanical behavior of plate's structures (Dastjerdi and Akgöz 2018). However, this method is so difficult especially for analyzing the axisymmetric problems, in consequence, the quasi three-dimensional theories can be developed as well. Recently, the plate theories have been used widely to model the mechanical behavior of macro and nano plate's structures (Chaubey, Kumar, and Chakrabarti 2018; Dastjerdi, Akgöz, and Yazdanparast 2018; Dastjerdi and Tadi Beni 2019; Dastjerdi, Akgöz, and Civalek 2020; Li 2017; Karami, Janghorban, and Li 2018; Karami, Janghorban, and Tounsi 2019; Karami, Janghorban, and Rabczuk 2019a, 2019b; Matsunaga 2004, 2008a; 2008b; 2009; Jena, Chakraverty, Malikan, and Tornabene 2020; Malikan, Jabbarzadeh, and Dastjerdi 2017; Malikan 2017, Malikan and Eremeyev 2020), however, these theories cannot be applied to study the thick and very thick structures because of neglecting the strain changes along the thickness. Wu, Chiu, and Wang (2011) examined a quasi-three-dimensional analysis of simply supported, multilayered composite and FGM plates with developing a meshless collocation (MC) and an element-free Galerkin method and with using the differential reproducing kernel (DRK) interpolation. Alibeigloo (2011) studied the vibration analysis of a nanoplate based on the three-

dimensional theory of elasticity using nonlocal continuum mechanics. Mantari and Soares (2012) presented a generalized hybrid quasi-three-dimensional shear deformation theory for the bending analysis of FG Plates with six unknowns. Neves et al. (2012a) derived a quasi-three-dimensional hyperbolic sine shear deformation theory for the bending and free vibration analysis of FG plates. Neves et al. (2012b) investigated the bending and free vibration and also deformations of FG plates using a quasi-three-dimensional sinusoidal shear deformation theory. Thai and Kim (2013) presented a quasi-three-dimensional theory for the bending analysis of functionally graded plates with considering both shear deformation and thickness stretching effects by a sinusoidal variation of all displacements through the thickness. Thai et al. (2014) developed a quasi-three-dimensional hyperbolic shear deformation theory for bending and vibration of FG plates with five unknowns. Neves et al. (2013) also presented a quasi-three-dimensional HSDT for modeling FG plates accounting for extensibility in the thickness direction. Mantari and Soares (2014) presented a quasi-three-dimensional HSDT with four unknowns for the static analysis of advanced composite plates. The governing equations and boundary conditions are derived by employing the principle of virtual work. Mantari and Granados (2017) also formulated an analytical solution for the thermo-elastic bending analysis of advanced composite sandwich plates by using a quasi-three-dimensional hybrid type HSDT with six unknowns. Jin et al. (2015) investigated the free vibration behaviors of FG sector plates with using three-dimensional theory of elasticity. Bessaim et al. (2015) presented a nonlocal quasi-three-dimensional trigonometric plate theory for micro/nanoscale plates. In order to introduce the size influences, the Eringen's nonlocal elasticity theory was utilized with using five unknowns in FSDT. Mahmoudi et al. (2017) presented a quasi-three-dimensional shear deformation theory for thermo-mechanical analysis of FG sandwich plates resting on a Pasternak elastic foundation. The number of unknowns and governing equations of the presented theory was four and was derived with using the principle of virtual displacements and also the stretching effect was considered due to its quasi-three-dimensional nature. Nguyen et al. (2017) investigated a novel quasi-three-dimensional seventh-order shear deformation theory with four unknowns in order to investigate size-dependent behaviors of FG microplates with using the modified couple stress theory (MCST) for bending, free vibration and buckling responses of the rectangular and circular functionally graded microplates and they considered both shear deformations and thickness stretching effect without requiring shear correction factors. Adhikari and Singh (2018) presented a higher order quasi three-dimensional theory for free and forced vibration of laminated composite plates. Nikbakht et al. (2017) investigated the elastic bending of FG plates up to yielding with using the full layer-wise method and they compared the numerical results with the results obtained from quasi three-dimensional elasticity and various shear deformation theories. Farzam-Rad, Hassani, and Karamodin (2017) presented a quasi-three-dimensional shear deformation theory for the static and free vibration analysis of functionally graded and sandwich plates by using the isogeometric analysis (IGA) method and physical neutral surface position. Recently Liu et al. (2017) modeled a new plate formulation by using the characteristics of the IGA in combination with a quasi-three-dimensional hyperbolic shear deformation theory for bending, vibration and buckling of FG Plates with five unknowns. Bouafia et al. (2017) studied bending and free vibration behaviors of FG nanobeams using a nonlocal quasi-three-dimensional theory that can capture the small-scale effect, and furthermore accounts for both shear deformation and thickness stretching effects by virtue of a hyperbolic variation of all displacements through the thickness without using shear correction factors. Benahmed et al. (2017) developed a quasi-three-dimensional hyperbolic shear deformation theory for bending and vibration analyses of FG plates resting on two-parameter elastic foundation that deals five

unknowns as the FSDT. Patil, Kant, and Desai (2018) presented a semi analytical approach by using three-dimensional (3-D) elasticity solution for simply supported FG material plate with exponential gradation of material properties. Zenkour (2018) developed the bending responses of porous FG single-layered and sandwich thick rectangular plates with using a refined quasi-three-dimensional shear and normal deformation theory. Abualnour et al. (2018) presented a quasi-three-dimensional trigonometric shear deformation plate theory for free vibration of FG plates with only five unknowns. Malikan, Tornabene, and Dimitri (2018) investigated a linear three-dimensional elasticity analysis for a thick nanoplate with considering functionality and porosity in order to study stability conditions. They solved the achieved linear equations based on the analytical solution methods. Shahsavari et al. (2018) studied a new quasi three-dimensional elasticity theory based on a hyperbolic function in order to consider natural frequencies of a functionally graded plate by assuming porosities. The plate was also assumed to be rested on the Winkler-Pasternak matrix. There have also been done some other crucial research on the plates based on the three-dimensional elasticity theory (Karami et al. 2018). To the sake of the brevity, the other important research done on the nanostructures are found by (Karami et al. 2019; Dastjerdi and Akgöz 2019).

In this paper, it is tried to find a solution for obtaining the approximate results of exact three-dimensional elasticity theory (3D) for an annular/circular FGM rotating disk in hygro-thermal environment. The disk is considered to have porosity as structural defect. The complexity of the exact 3D theory has been reduced in applied theories. This aim has been achieved by considering the variations of strain along the thickness as a changeable polynomial function. In addition, another simpler quasi three-dimensional theory has been developed. By this strategy, if the three-dimensional analysis is intended for a sector-shaped plate, three independent variables r, θ and z have been reduced to only r and θ. And if a symmetric problem like annular/sector plate under uniform loading is considered, two variables r and z will be reduced to only r. In other words, in case of symmetric annular /circular plate, the approximate results of 3D will be obtained only by solving the set of ordinary differential equations which are significantly simpler than partial differential equations. In summary, the applied theories reduce the complexity of the exact three-dimensional theory dramatically with the same accuracy.

2. Governing equations

One of the biggest challenges faced by researchers and engineers is solving the differential equations. If the number of variables is greater than two, for example, there are three independent variables, solving a system of partial differential equations with three independent variables is usually very difficult (If not impossible especially in nonlinear analysis). Solving methods for this category of problems are often associated with a lot of difficulties, which often enforces researchers to simplify the three independent variables into two variables. Even a numerical or semi-analytical solution for partial differential equations system with two variables has usually complexities, which is time-consuming and requires complex programming, but is still solvable. Many of the mechanical analytical issues fall into this category.

In this paper, we are faced with a problem in the mechanics of very thick structures in which many researchers are involved as a challenge, and each researcher considers a method for solving the governing equations. The 3D analysis of structures so that the variations along the thickness are taken into account, is always a challenge for researchers. Considering strain changes along the thickness results in higher precision of the results, especially in the case of thick and very thick structures that are affected by hygro-thermal environments (Dastjerdi and Akgöz 2018). In the

mentioned cases, ignoring the strain along the thickness (ε_z) leads to very serious errors. So, the problem ahead is to consider these changes (ε_z) in the direction of thickness (h). The geometry of the plate is considered as an annular/circular FGM rotating disk (with constant rotating velocity □) under transverse loading q (r) that is embedded in Winkler-Pasternak (k_w, k_p) elastic matrix (**Figure 1**). It is noted that for ω □ 0 the elastic foundation must be eliminated due to the rotation of structure.

Figure 1. Symmetric annular/circular FGM rotating disk embedded in Winkler-Pasternak elastic foundation under transverse loading q (r)

2.1. Exact three-dimensional elasticity theory

In the case of the axisymmetric problem (eliminating the changes along θ direction), there are three independent variables r, θ and z. According to the above description, solving a system of partial differential equations with three independent variables is very difficult. Here, a sector sheet is considered as shown in **Figure 2**. The solid black circles are nodes on the boundaries that the values of independent displacement field variables are determined by boundary conditions, and the points represented by a hollow circle obey the governing equations.

If the displacement field is considered as $u(r, \theta, z)$, $v(r, \theta, z)$, and $w(r, \theta, z)$, the three independent governing equations in static state can be formulated as follows:

$$\delta u : \frac{\partial \sigma_r}{\partial r} + \frac{1}{r}\frac{\partial \sigma_{r\theta}}{\partial \theta} + \frac{\partial \sigma_{rz}}{\partial z} + \frac{1}{r}\left(\sigma_r - \sigma_\theta\right) = 0 \tag{1}$$

$$\delta v : \frac{\partial \sigma_{r\theta}}{\partial r} + \frac{1}{r}\frac{\partial \sigma_\theta}{\partial \theta} + \frac{\partial \sigma_{\theta z}}{\partial z} + \frac{2}{r}\sigma_{r\theta} = 0 \tag{2}$$

$$\delta w : \frac{\partial \sigma_{rz}}{\partial r} + \frac{1}{r}\frac{\partial \sigma_{\theta z}}{\partial \theta} + \frac{\partial \sigma_z}{\partial z} + \frac{1}{r}\sigma_{rz} = 0 \tag{3}$$

where σ_{ij} denotes the tensor of static stresses on an element of the plate. Now, if it is aimed to analyze the problem in the situation by considering $\varepsilon_z \neq 0$, to avoid the large number of equations and the insolubility of the equation system, the geometry of the problem is assumed as an annular/circular under the uniform loading. Consequently, due to symmetric problem the changes in θ direction will be eliminated. According to **Figure 3**, only the changes in r and z will be obtained.

Figure 2. Three-dimensional schematic view of a sector FGM plate in r, θ and z directions

Figure 3. An annular/circular FGM plate under uniform loading (q_z)

According to the grid point distribution, there are number of five nodes in r and z directions. Consequently, the number of 2×25 = 50 equations will be obtained that can be solved conveniently as the authors of the present paper already studied in their previous paper (Dastjerdi and Akgöz

2018). The governing equations can be concluded from Eqs. (1-3) as follows (By neglecting the changes in θ direction):

$$\delta u : \frac{\partial \sigma_r}{\partial r} + \frac{\partial \sigma_{rz}}{\partial z} + \frac{1}{r}\left(\sigma_r - \sigma_\theta\right) = 0 \tag{4}$$

$$\delta w : \frac{\partial \sigma_{rz}}{\partial r} + \frac{\partial \sigma_z}{\partial z} + \frac{1}{r}\sigma_{rz} = 0 \tag{5}$$

In this case, the theory of exact three-dimensional elasticity is considered and the obtained results are highly accurate. Solving the set of Eqs. (4, 5) is not a complex task because there are only two independent variables *r* and *z*. However, if analysis of an axisymmetric problem is intended, an appropriate solution method should be applied in order to improve the accuracy of the exact three-dimensional analysis. Whereas, the set of third-order partial differential equations are derived based on Eqs. (1-3) which is extremely complex.

For example, if a numerical method such as the differential quadrature method (DQM) or the semi-analytical polynomial method (SAPM) is applied, it is required to solve 9×9×2 = 162 equations and 162 unknowns according to Eqs. (4-5). If Eqs. (1-3) are used that consider changes along θ direction, the number of 9×9×9×3 = 2187 equations and 2187 unknowns will be achieved. Because of the massive calculations, the solving process will be remarkably time-consuming and even impossible for ordinary computers. Consequently, a super computer is needed for this issue which increases the research costs significantly.

2.2. Quasi three-dimensional elasticity theory

In this paper, two effective quasi three-dimensional theories have been used in order to resolve the shortcomings of exact three-dimensional elasticity theory. One of the mentioned shortcomings is deriving a large number of governing equations which are higher-order partial differential equations. The quasi three-dimensional theories eliminate the disadvantages of exact three-dimensional theory by reducing the number of equations, while providing a very good performance and accuracy with respect to the comparison of the results with the exact three-dimensional analysis.

2.2.1. CUF quasi three-dimensional elasticity theory

Firstly, the CUF (Carrera's Unified Formulation) displacement field for a thick sector plate as shown in **Figure 2** can be expressed as follows (Carrera et al. 2011):

$$U\left(r,\theta,z\right) = \sum_{i=1}^{k} u_i\left(r,\theta\right) \times z^{(i-1)} \tag{6}$$

$$V\left(r,\theta,z\right) = \sum_{i=1}^{k} v_i\left(r,\theta\right) \times z^{(i-1)} \tag{7}$$

$$W\left(r,\theta,z\right) = \sum_{i=1}^{k} w_i\left(r,\theta\right) \times z^{(i-1)} \tag{8}$$

where U, V, and W are displacements of the plate along *r*, θ, and *z* directions, respectively. Moreover, *z* defines the thickness coordinate. If the symmetric annular/circular plate is considered according to **Figure 1**, the displacement field for this theory will be defined as the following relations (there are not any changes in θ direction, in consequence, $V(r, \theta, z) = 0$).

$$U(r,z)=\sum_{i=1}^{k}u_i(r)\times z^{(i-1)} \tag{9}$$

$$W(r,z)=\sum_{i=1}^{k}w_i(r)\times z^{(i-1)} \tag{10}$$

Because of symmetry in the geometry, there are no changes along θ direction and functions u_i and w_i (i = 1..k) are only a function of variable r. High amount of k leads to the high precision for simulation of very thick sheets in a way that the obtained results of the proposed theory can be compared with the exact three-dimensional analysis with a high level of accuracy and low differences. However, less orders can be considered too (for example, third-order). Regarding Eqs. (9, 10), there are number of 12 unknowns for functions u_i and w_i (k = 6), and it is expected that the number of 12 ordinary differential equations would be obtained (since changes are only in r direction). Now, in order to obtain the governing equations for an annular/circular FGM rotating disk under uniform loading in hygro-thermal environment, the strain fields are considered as the following relations (considering Von Kármán's assumptions):

$$\varepsilon_r=\frac{dU}{dr}+\frac{1}{2}\left(\frac{dW}{dr}\right)^2-\alpha(z)\cdot\Delta T-\beta(z)\cdot\Delta H \tag{11}$$

$$\varepsilon_\theta=\frac{U}{r}-\alpha(z)\cdot\Delta T-\beta(z)\cdot\Delta H \tag{12}$$

$$\varepsilon_z=\frac{dW}{dz}+\frac{1}{2}\left(\frac{dW}{dz}\right)^2-\alpha(z)\cdot\Delta T-\beta(z)\cdot\Delta H \tag{13}$$

$$\varepsilon_{rz}=\frac{dU}{dz}+\frac{dW}{dr} \tag{14}$$

$$\varepsilon_{r\theta}=\varepsilon_{\theta z}=0 \tag{15}$$

where ε_{ij} exhibits the field of static strains. One of the atmospheric parameters involved in industrial environments may be the humidity that an efficiency of a machine may be related to it. High or low humidity in the air, depending on the type of machine operating in the environment. Too much moisture can lead to improper machining and disturbances in machinery, indicating the importance of examining the humidity in mechanical behavior of materials. Hence, in this paper these two important factors are considered in the analysis. As it can be seen in the above equations, the thermal and hygral effects are considered in relations. $\alpha(z)$ and $\beta(z)$ are the thermal conductivity and hygral expansion along the thickness. ΔT and ΔH are the temperature differences and moisture concentration (Malikan and Nguyen 2018). The material properties of the plate are considered as functionally graded material (FGM) which is the Young's modulus varies from metal to ceramic along the thickness (vice versa is possible too). Ceramic side of the plate is under the loading. The Young's modulus variations can be formulated as follow:

$$E(z)=E_m+(E_c-E_m)\left(\frac{1}{2}+\frac{z}{h}\right)^g-\frac{\lambda}{2}(E_c+E_m) \tag{16}$$

$$E(z)=E_m+(E_c-E_m)\left(\frac{1}{2}+\frac{z}{h}\right)^g-\frac{\lambda}{2}(E_c+E_m)\left(1-\frac{2|z|}{h}\right) \tag{17}$$

$$\alpha(z)=\alpha_m+(\alpha_c-\alpha_m)\left(\frac{1}{2}+\frac{z}{h}\right)^g \tag{18}$$

In which, E_c and E_m are the ceramic and metal amounts of Young's modulus. Parameter g represents to the variation's rate from ceramic to metal property. More value of g, the steeper slope of variations from metal to ceramic property. Porosity makes a different response for the model. So, it can be highly recommended to be taken into account such a manufacturing defect. In which λ denotes the type of porosities distribution. The even porosity is illustrated by Eq. (16) and the uneven porosity relation is expressed by Eq. (17). The porosity parameter is in fact the focus of many sciences including many branches of engineering and is very important for achieving other important parameters. Therefore, the studying and understanding how porosity affects and its types can be important. The relation between stress and strain can be seen below (□is Poisson ratio):

$$\sigma=C:\varepsilon \tag{19}$$

$$C=\begin{bmatrix} \frac{E(z)(1-\nu)}{(1-2\nu)(1+\nu)} & \frac{E(z)\nu}{(1-2\nu)(1+\nu)} & \frac{E(z)\nu}{(1-2\nu)(1+\nu)} & 0 \\ \frac{E(z)\nu}{(1-2\nu)(1+\nu)} & \frac{E(z)(1-\nu)}{(1-2\nu)(1+\nu)} & \frac{E(z)\nu}{(1-2\nu)(1+\nu)} & 0 \\ \frac{E(z)\nu}{(1-2\nu)(1+\nu)} & \frac{E(z)\nu}{(1-2\nu)(1+\nu)} & \frac{E(z)(1-\nu)}{(1-2\nu)(1+\nu)} & 0 \\ 0 & 0 & 0 & \frac{E(z)}{2(1+\nu)} \end{bmatrix} \tag{20}$$

$$\varepsilon=\begin{bmatrix}\varepsilon_r & \varepsilon_\theta & \varepsilon_z & \varepsilon_{rz}\end{bmatrix}^T \tag{21}$$

where the Poisson's ratio is depicted by ν and assumed to be constant in the thickness direction. The governing equations have been derived based on the stationary of minimum potential energy. Which U_p is the potential energy due to the internal stresses, and Ω is the work of external imposed forces like loading and foundation. According to the minimum potential energy principle for the static analysis, the variations of internal and external energies must be zero as follow:

$$\begin{aligned} &\delta U_p+\delta\Omega=0 \\ &\iiint_V\left(\sigma_r\delta\varepsilon_r+\sigma_\theta\delta\varepsilon_\theta+\sigma_z\delta\varepsilon_z+\sigma_{rz}\delta\varepsilon_{rz}\right)dV+\iint\left(q_z+k_wW-k_p\nabla^2W\right)rdrd\theta\delta W=0 \\ &\nabla^2=\left(\frac{d^2}{dr^2}+\frac{1}{r}\frac{d}{dr}\right) \end{aligned} \tag{22}$$

in which the external loads are respectively the lateral uniform load, Winkler module and the shear layer of the foundation as q_z, k_w, and k_p. It is assumed that the structure rotates with the constant rotating velocity ω (**Figure 1**). After applying integrations and mathematical calculations, the governing equations can be derived. The obtained governing equations and stress resultants are presented in appendix (A.1).

In this paper, all types of boundary conditions including the free edges are considered. So, the boundary conditions when □ = 0 can be expressed as follows:

$$\begin{cases} \text{Clamped (C):} & \begin{cases} u_1 = u_2 = u_3 = u_4 = u_5 = u_6 = 0 \\ w_1 = w_2 = w_3 = w_4 = w_5 = w_6 = 0 \end{cases} & R_i, R_o \\ \text{Simply Supported (S):} & \begin{cases} u_1 = M_r = P_r = H_r = Y_r = S_r = 0 \\ w_1 = w_2 = w_3 = w_4 = w_5 = w_6 = 0 \end{cases} & R_i, R_o \\ \text{Free Edge (F):} & \begin{cases} N_r = M_r = P_r = H_r = Y_r = S_r = 0 \\ Q_{rz} = M_{rz} = P_{rz} = H_{rz} = Y_{rz} = S_{rz} = 0 \end{cases} & R_i, R_o \end{cases} \tag{23}$$

Also, the definition for clamped and free boundary conditions for a rotating disk are the same as formulation in Eq. (42). There is another boundary condition entitled roller supported. It is noted that the inner radius can only have clamped and roller supported and the outer radius might have the free and roller supported conditions respectively.

$$\text{Roller Supported (RS):} \begin{cases} N_r = M_r = P_r = H_r = Y_r = S_r = 0 \\ w_1 = w_2 = w_3 = w_4 = w_5 = w_6 = 0 \end{cases} \quad R_i, R_o \tag{24}$$

The boundary conditions CRS means that the inner radius of the plate (r_i) is clamped and the outer radius (r_o) is roller supported.

2.2.2. Simplified quasi three-dimensional elasticity theory

As mentioned before, another simpler theory has been presented in this paper in order to simulate the very thick FGM rotating disk. The mentioned quasi three-dimensional formulations (appendix (A.1)) reduces the number of orders into set of differential equations and gives the approximate results of the exact three-dimensional elasticity. This is certainly the advantage of proposed methodology. However, it has an obvious shortcoming which is the high number of obtained equations (number of 8 and 12 equations for third and fifth-order polynomial expansions). Due to the mentioned shortcoming, the authors applied another simplified quasi three-dimensional theory (abbreviated as SQT) in which its displacement fields are formulated as follow:

$$U(r,z) = u_1(r) + f(z)u_2(r) \tag{25}$$

$$W(r,z) = w_1(r) + g(z)w_2(r) \tag{26}$$

The functions *f*(*z*) and *g*(*z*) are arbitrary. They selected in a way that the desirable accuracy of the results is obtained. As it can be seen, there are only number of four unknowns in the displacement field as u_1, u_2, w_1 and w_2. Consequently, it is expected that the total number of four governing equations will be derived. The process for deriving the governing equations is the same as deriving the proposed equations in appendix A.1. The linear strains can be formulated as follow:

$$\varepsilon_r = \frac{du_1}{dr} + f(z)\frac{du_2}{dr} - \alpha(z)\cdot\Delta T - \beta(z)\cdot\Delta H \tag{27}$$

$$\varepsilon_\theta = \frac{1}{r}\left(u_1 + f(z)u_2\right) - \alpha(z)\cdot\Delta T - \beta(z)\cdot\Delta H \tag{28}$$

$$\varepsilon_z = \left(\frac{d}{dz} g(z)\right) w_2 - \alpha(z) \cdot \Delta T - \beta(z) \cdot \Delta H \tag{29}$$

$$\varepsilon_{rz} = \left(\frac{d}{dz} f(z)\right) u_2 + \frac{dw_1}{dr} + g(z) \frac{dw_2}{dr} \tag{30}$$

$$\varepsilon_{r\theta} = \varepsilon_{\theta z} = 0 \tag{31}$$

The resulted governing equations can be derived by using the above strain field according to energy method. The governing equations including the stress resultants are presented in appendix A.2 based on the simplified quasi three-dimensional theory (SQT). Also, the boundary conditions can be defined as follows:

$$\begin{cases} \text{Clamped (C):} & \begin{cases} u_1 = u_2 = 0 \\ w_1 = w_2 = 0 \end{cases} \quad R_i, R_o \\ \text{Simply Supported (S):} & \begin{cases} u_1 = P_r = 0 \\ w_1 = w_2 = 0 \end{cases} \text{ Roller Supported (RS):} \begin{cases} N_r = P_r = 0 \\ w_1 = w_2 = 0 \end{cases} \quad R_i, R_o \\ \text{Free Edge (F):} & \begin{cases} N_r = P_r = 0 \\ N_{rz} = P_{rz} = 0 \end{cases} \quad R_i, R_o \end{cases} \tag{32}$$

3. Solving process

There are many challenges with solving nonlinear partial differential equations for researchers who work on the mechanical behavior of nonlinear systems. Presenting an efficient method that gives suitable outcomes in a simpler way is always desirable for mechanics' scholars. The idea of a solution method based on polynomial functions has long been common. However, in this work, these polynomials are introduced in general so that there is no need to be initially satisfied the boundary conditions and the boundary conditions would be applied on these polynomials in the solution process. To give an example, if we assume the geometry of the problem as a sector, the variables are in line with r and θ. As can be observed by **Figure 4**, M=N=5 is chosen and generally we obtain 5×5 nodes. Thus, the number of coefficient functions for SAPM would be 25 of which 16 nodes are located on the borders and 9 nodes are placed in the grid which obey the governing equations. The required SAPM function is here in the following form:

$$f(r,\theta) = \sum_{i=1}^{N} \sum_{j=1}^{M} a_{\left(i+j-(1-(i-1)(M-1))\right)} r^{(i-1)} \theta^{(j-1)} \quad (N = M = 5) \tag{33}$$

Figure 4. Sample grid points for a sector

Now, the aforesaid function (Eq. (33)) can be replaced with the partial differential governing equations of the problem and hence, the partial differential equations will be transformed to a set of algebraic equations. Now, by applying 16 algebraic equations related to the boundary conditions and 9 algebraic equations related to the internal nodes of the grid, 25 governing equations will be attained that regarding 25 unknown variables ($a_i = 1..25$), the function $f(r,\theta)$ will be harvested

and the problem can be solved conveniently by using a numerical method (for example Newton-Raphson method).

In this paper, based on the above mentioned points, due to the efficiency and simplicity of the SAPM solving method, this method has been used to solve the governing differential equations. Applying this method for quasi three-dimensional analysis is original and has been used only in this research. The SAPM functions are presented for the current problem as follows:

$$u_j = \sum_{i=1}^{N} a_{(i+(j-1)\times N)} r^{(i-1)} \qquad j = 1..6 \tag{34}$$

$$w_j = \sum_{i=1}^{N} a_{(i+6N+(j-1)\times N)} r^{(i-1)} \qquad j = 1..6 \tag{35}$$

where r is the variable of radius. Now with substitution the above equations into the governing equations, the differential equations will be transformed to the algebraic equations as mentioned before. For example, the expression for ε_r (in Eq. (11)) can be written as follow (Applying SAPM functions):

$$\begin{aligned}
\varepsilon_r = \frac{\partial U}{\partial r} + \frac{1}{2}\left(\frac{\partial W}{\partial r}\right)^2 - \alpha(z)\cdot\Delta T - \beta(z)\cdot\Delta H = \frac{d}{dr}\sum_{i=1}^{N} a_i r^{(i-1)} + z\,\frac{d}{dr}\sum_{i=1}^{N} a_{(i+N)} r^{(i-1)} \\
+ z^2\frac{d}{dr}\sum_{i=1}^{N} a_{(i+2N)} r^{(i-1)} + z^3\frac{d}{dr}\sum_{i=1}^{N} a_{(i+3N)} r^{(i-1)} + z^4\frac{d}{dr}\sum_{i=1}^{N} a_{(i+4N)} r^{(i-1)} + z^5\frac{d}{dr}\sum_{i=1}^{N} a_{(i+5N)} r^{(i-1)} \\
+ \frac{1}{2}\left(\frac{d}{dr}\sum_{i=1}^{N} a_{(i+6N)} r^{(i-1)} + z\,\frac{d}{dr}\sum_{i=1}^{N} a_{(i+7N)} r^{(i-1)} + z^2\frac{d}{dr}\sum_{i=1}^{N} a_{(i+8N)} r^{(i-1)} + z^3\frac{d}{dr}\sum_{i=1}^{N} a_{(i+9N)} r^{(i-1)}\right. \\
\left. + z^4\frac{d}{dr}\sum_{i=1}^{N} a_{(i+10N)} r^{(i-1)} + z^5\frac{d}{dr}\sum_{i=1}^{N} a_{(i+11N)} r^{(i-1)}\right)^2 - \alpha(z)\cdot\Delta T - \beta(z)\cdot\Delta H
\end{aligned} \tag{36}$$

For the rest of the equations, the process is similar to Eq. (36). The more details for SAPM methodology can be found in the author's previous papers as (Dastjerdi, Akgöz, and Civalek 2020).

4. Results and discussions

First, the comparison between the results of applied theory with eight and twelve unknowns (the third and fifth-order) is presented in **Table 1**. From now the applied quasi three-dimensional theory is considered the CUF quasi three-dimensional theory (abbreviated as CUFQT). There are dramatic differences for the program runtime between the third and fifth-order theories especially for axisymmetric problems. Of course, the time which is spent for third-order theory is much shorter than the fifth-order. But the problem is the accuracy of the obtained results which are presented in **Table 1**. For more consideration, the third and fifth-order displacement fields of CUFQT are presented as follows:

$$\text{Third-order}\begin{cases} U(r,z) = \sum_{i=1}^{4} u_i(r)\times z^{(i-1)} \\ W(r,z) = \sum_{i=1}^{4} w_i(r)\times z^{(i-1)} \end{cases} \quad \text{Fifth-order}\begin{cases} U(r,z) = \sum_{i=1}^{6} u_i(r)\times z^{(i-1)} \\ W(r,z) = \sum_{i=1}^{6} w_i(r)\times z^{(i-1)} \end{cases} \tag{36}$$

Table 1 gives the results for different values of thickness (h) and loading. Parameter R_{TF} is the difference between the results of third and fifth-order theories. As concluded, the differences between the results of third and fifth-order theories are so inconsiderable for small amounts of thickness and the result are approximately similar (99.9% similarity). The amount of loading does not affect the results in comparison with the thickness. Parameter R_{TF} is about 96% and there is only 4% difference for very thick plates. So, it is recommended to apply the fifth-order CUFQT for very thick structures. In summary, it is possible to use the third-order CUFQT for thick plates that gives the very similar results to the fifth-order CUFQT in very shorter time. Due to obtain the more accurate results, the fifth-order CUFQT will be used for the rest of investigations in this paper.

First, it is needed to compare the obtained results of the CUFQT in this study with the results of other available articles. Therefore, in **Table 2** and **Table 3**, it can be seen the comparison between the results of this study and other articles in **Table 2**, and comparison with the results of ABAQUS software in **Table 3**. Parameter R_{AP} presents the ratio between the results of ABAQUS software to the obtained results of the present paper (P.P) and R_{TP} is the ratio between the results of TSDT analysis to the present paper. As it can be seen in **Table 2**, the results of the CUFQT are very close to the results of the exact three-dimensional elasticity theory. For different values of h/a, this suitable agreement can be seen between the results. According to **Table 2**, it is concluded that the increase in the parameter related to the functional property of the FGM substance does not affect the accuracy and convergence of the results. But with increasing the structure thickness, the results of exact three-dimensional elasticity theory and the CUFQT are closer to each other. Therefore, according to **Table 2**, the results of the CUFQT can be fully utilized. In **Table 3**, the comparison between the results of the CUFQT and ABAQUS software as well as the results of the TSDT theory can be seen for different thicknesses. Also, the results for the two FC and CC boundary conditions are presented. According to **Table 3** for FC boundary conditions, with the increase in the thickness, the results of the present study are closer to the results of ABAQUS software. Also, the results of the present paper are always less than the results of ABAQUS. This conclusion can be seen in the case of CC boundary conditions, but here the results of the present research and ABAQUS are closer to each other. But in general, the difference between the results of the CUFQT and ABAQUS is not so significant, however the difference between the results of the CUFQT and the theory of TSDT for higher amounts of thickness is very significant. For example, this difference for the FC boundary conditions and the thickness $h = 1m$ is about 36%, but this difference is about 100% for the boundary conditions CC and the thickness $h = 1m$, which is very high and therefore the results of TSDT for large thicknesses cannot be used at all. All of the plate theories eliminate the strain through the thickness. On the other hand, the amount of ε_z is zero for plate theories including TSDT. This assumption ($\varepsilon_z = 0$) is acceptable for thin and moderately thick plates. However, the amounts of deflection for a thick plate can be different for lower and upper surfaces of the plate (**Figure 3**) because by neglecting ε_z only a single value for deflection will be obtained (for CLPT, FSDT and TSDT analyses). For example, the upper surface in **Figure 3** which is under the transverse loading has more deflection in comparison with the lower surface which is not under the loading. Consequently, the results of three-dimensional analysis for very thick plates are significantly different in comparison with the results of plate theories such as TSDT. The greater difference between the results of ABAQUS software and the CUFQT in lower thicknesses can be attributed to the nonlinear analysis (large deformation analysis) in this paper. It can be assumed that the results of the CUFQT are even more accurate than the finite element

analysis of ABAQUS software. Moreover, the thicker the plate, the closer the results of two analyzes, especially in the more rigid boundary conditions (CC).

Table 1. The results of the third and fifth-order CUFQT for different values of thickness and load

Table 2. Comparison between the CUFQT results of present paper (P.P) and the exact three-dimensional results in (Dastjerdi, and Akgöz 2018)

Table 3. Validation of the results of present paper (CUFQT) with ABAQUS and TSDT analysis for different values of thickness and boundary conditions

As explained in the solving process section, in this paper a highly efficient method (SAPM) is used to solve the governing equations. To examine the convergence rate of this method, **Figure 5** shows the CUFQT results versus the number of nodes in the geometry range of the analyzed sheet. Changes for the two CUFQT and the exact three-dimensional elasticity theory are presented. As it can be seen, the rate of convergence for the CUFQT is much higher than the exact three-dimensional elasticity theory. So that only by choosing three nodes, the CUFQT results converge up to 80% which is only 60% for the exact three-dimensional theory. In the CUFQT, the convergence up to 98% is achieved by only selecting five nodes and the convergence is approximately 99.7% with the selection of seven nodes. But for the exact three-dimensional theory, it is necessary to consider nine nodes in order to obtain reliable results which means it is required to spend more time on the solution process. Therefore, according to the obtained results in **Figure 5**, the convergence rate of the CUFQT is much higher than the exact three-dimensional theory. This is one of the most important benefits of applying the CUFQT analysis.

Figure 5. The rate of convergence for the results of CUFQT and the exact three-dimensional elasticity theory

In **Figure 5**, the convergence rate of solution method for the two CUFQT used in this paper and the exact three-dimensional theory is investigated. Now the time duration that is spent for obtaining the results (for computer program) is discussed in **Table 4**. Definitely the overall obtained time depends on the type of computer which is used. In this paper, a typical Corei7 Laptop is used. Parameter R_{PE} shows the difference between the results of present paper and the exact three-dimensional theory. The data in **Table 4** represent the runtime (computer program) for different number of nodes for the two theories of exact three-dimensional and CUFQT. **Table 4** shows the changes for the two boundary conditions CC and SS. For nodes below three and five, the runtime for the exact three-dimensional theory is less than the CUFQT. But according to the results obtained in **Figure 5**, the selection of lower node numbers does not provide the necessary convergence for the exact three-dimensional theory results, and it is necessary to select nine nodes to obtain a reliable result. In this case the runtime of the program for the exact three-dimensional theory is above eighty seconds. The same result for the CUFQT (with the same number of nodes) is about twenty seconds, which is four times lower than the exact three-dimensional theory. Regard to the CUFQT, selection of seven nodes gives reliable results. This will take less time to run the computer program. It should be noted that the studied geometry is a symmetric annular/circular

FGM rotating disk. In the theory of CUFQT, displacement field only depends on *r* direction and in the exact three-dimensional theory, changes are in *r* and *z* directions. For the CUFQT, the governing equations are ordinary differential equations and the relations extracted from the exact three-dimensional theory are the second-order partial differential equations. Now, if a sector sheet is considered, the governing equations will be the second-order partial differential equations for the CUFQT and third-order for the exact three-dimensional theory. For a set of third-order partial differential equations, its solution is very time-consuming if it is not impossible to be solved especially for the nonlinear analysis. But, as it was seen, the second-order partial differential equations obtained from the CUFQT can be solved conveniently. So, by using the CUFQT the set of third-order partial differential equations will be converted into the second-order one. Applying this method is so recommended while the strain changes through the thickness is considerable (thick and especially very thick plates). So that the obtained results are very similar to the exact three-dimensional theory. Also, according to **Table 4**, it can be concluded that the choice of different types of boundary conditions does not affect the runtime for program, and almost the solution speed will be approximately similar for the different types of boundary conditions.

Table 4. Runtime for present paper (CUFQT) and the exact three-dimensional elasticity theory for different types of boundary conditions and node numbers

An annular/circular FGM disk is considered with the following specifications. The rotating velocity is zero ($\omega = 0$). The boundary conditions are clamped for both inner and outer radiuses (CC).

$$\begin{aligned} &r_i = 0.2m; r_o = 1m; h = 0.5m; E_m = 1.9\times10^{11}Pa; E_c = 0.85\times10^{11}Pa; \nu = 0.29 \\ &g = 5; q_z = 0.1GPa; \Delta H = \Delta T = 0 \end{aligned} \tag{37}$$

The material in this study is considered a type of functionally graded material (FGM). First, variations of deflection along the thickness for different values of *g* (slope rate of metal to ceramic change) are studied in **Figure 6**. In the case of $g = 0$, the material property is only pure metal, and it is observed that the slightest increase is obtained in this case. By increasing the amount of *g*, the deflection is intensified. But it is observed that at the beginning of the incremental trend, the growth of deflection is sharper. But as *g* increases, this incremental rate decreases. The other issue is the amount of variation through the thickness (*z*). By increasing the *g* value, the deflection along the thickness increases. Therefore, the higher the ceramic property of the material, the higher the rate of deflection change along the thickness. So, the use of three-dimensional theory is further enhanced. In the analysis of thick FGM sheets, it is recommended to use theories in which ε_z is not zero, especially for high values of *g*. Given the simplicity and similar results of the exact three-dimensional theory, the use of CUFQT can be very efficient (According to the results of **Figure 6**).

Figure 6. The deflection along the thickness for different values of FGM parameter *g*

In this paper, the von Kármán's assumption which considers the large deformation has been used. Regarding the obtained governing equations, the presence of nonlinear terms can be observed. Using these assumptions will lead to more precise results (especially larger loads). Considering the nonlinear analysis, the number of calculations will increase dramatically. The nonlinear

relations (von Kármán's strain field) are considered in this paper due to obtaining as high as accurate results. The nonlinear analysis will be more important when the structure's thickness is small or high amounts of loading is attended. Actually, the amount of two parameters thickness and loading defines the threshold of large deformation. To aim comparing the results of three theories (CUFQT, SQT and the exact three-dimensional) for different values of loading, **Figure 7** is presented. **Figure 7 (a)** shows the changes for the load $q_z = 1$ GPa and **Figure 7 (b)** for $q_z = 10$ GPa. In linear analysis, as the load increases, the deflection increases with the same linear trend. For example, if the load is increased ten times, the deflection is exactly intensified ten times. But by comparing two graphs in **Figure 7 (a)** and **7 (b)**, it can be seen that with increasing the load from $q_z = 1$ GPa (**Figure 7 (a)**) to $q_z = 10$ GPa (**Figure 7 (b)**) the deflection does not grow ten times and will be less than this value. Here it can be seen the effects of nonlinear terms and the large deformation analysis. For example, the deflection increases from $0.0056m$ to $0.051m$, which show the increment approximately by nine times, not ten times (in the CUFQT analysis). Another point is the closer correspondence between the two theories of the exact three-dimensional and the CUFQT due to increase of applied loading. As the loading rises, the results of the two theories approach. So, for larger loads the results of both the exact three-dimensional and CUFQT theories can be used instead. The subject of closer approximation results in two theories is the number of nodes in each direction in the stage of solving the governing equations. According to **Figure 5**, the accuracy and convergence of results for CUFQT is more than the exact three-dimensional theory (especially for less amounts of node distribution). It is noteworthy that choosing the arbitrary functions $f(z)$ and $g(z)$ affects the obtained results of SQT analysis. For example, here $f(z) = g(z) = z^2 + z^3$. Another important conclusion according to **Figure 7** is good agreement between the results of CUFQT and SQT theories. There is only about 3% difference between the results of CUFQT and SQT. This amount of difference has been repeated in both **Figure 7** (a) and (b), in consequence, it is possible to use a correction factor in order to obtain the same results as CUFQT. As long as the number of governing equations in SQT analysis is less than the CUFQT (as mentioned before), it gives the results in shorter time. Eventually, due to the explained benefits of SQT it is recommended to apply this theory in three-dimensional analysis while it is needed to achieve a quick and moderately accurate result for thick and very thick structures. The other discussed conclusions regard to CUFQT are confirmed for SQT too because the entire trends for both CUFQT and SQT theories are the same and only a slight difference between the results can be observed.

(a) (b)

Figure 7. The results of CUFQT, SQT and the exact 3D theories for different values of loading (a) $q_z = 1$ GPa and (b) $q_z = 10$ GPa

One of the most important problems in analysis of plate structures that force researchers to use the three-dimensional elasticity theory is the high amount of thickness in which neglecting the ε_z causes the serious errors. The use of three-dimensional elasticity theory has many disadvantages that have already been addressed. Consequently, the authors of this study applied two suitable and efficient quasi three-dimensional theories that eliminates the disadvantages associated with the exact three-dimensional theory, however, the accuracy of the results is maintained. In **Figure 8** comparisons between the results of CUFQT, SQT and the three-dimensional elasticity theory for different thicknesses can be seen. As shown in **Figure 8**, the behavior of variations along the

thickness (z) for different thickness values for the three theories is the same. In both **Figures 8 a, b**, the results of SQT are less than the CUFQT and exact three-dimensional theory. But it is observed, the results of two theories (CUFQT and exact 3D) will be closer by increasing the thickness. The rate of approaching the results (as the thickness grows) has decreasing trend. Therefore (in high thicknesses), the results of the two theories (CUFQT and exact 3D) can be used more confidently instead. The thicker the sheet becomes, the greater the effect of using the three-dimensional elasticity theory. Therefore, according to **Figure 8**, the efficiency and closeness of the CUFQT and SQT results to the more precise exact three-dimensional elasticity theory are more evident (especially for more thicknesses). With regard to the results of **Figure 8**, it can be asserted that CUFQT and SQT (especially SQT) can be used for their many advantages, rather than the exact three-dimensional elasticity theory. Because of simplicity and shorter processing time, the use of quasi three-dimensional theories (CUFQT or SQT) is recommended instead of the exact three-dimensional elasticity.

(a) (b)

Figure 8. Comparison between the results of CUFQT, SQT and exact 3D theories for different values of thickness (a) h = 0.2m (b) h = 0.5m

Figure 9 shows the results of deflection through the thickness for different values of temperature by using the present study (CUFQT). The results at z = 0 are approximately equal for different values of the ambient temperature. However, the amount of deflection in z = (h / 2) and z = (-h / 2) will be different for several values of temperature and the slope of variations will be intensified with the increase of the temperature. Changes the deflection through-in thickness are almost linear, and the rate of change will be approximately linear. In other words, the rate of change, for example from $\Box T$ = 600 C^0 to $\Box T$ = 800 C^0, will be similar to $\Box T$ = 800 C^0 to $\Box T$ = 1000 C^0. Therefore, with variations in a certain temperature range (for other intervals) the approximate value of deflection through-in thickness can be predicted.

The sheet was analyzed under thermo-mechanical load, where $q_z = 1$ GPa (**Figure 9**). Now, if the sheet is only under a strict thermal load, it is possible to obtain the deflection changes along the thickness. If the plate theories such as CLPT, FSDT, TSDT or HSDT are used in analysis and the transverse load q_z on the sheet is zero, the deformation results will always be zero for different values of temperature. Because these theories essentially assume that strain variation along the thickness is zero ($\varepsilon_z = 0$). This is one of the biggest shortcomings of plate theories in thermo-mechanical analysis of plates. But since in this paper and the applied theory (CUFQT) ε_z is opposite to zero, for different values of temperature and $q_z = 0$, it can also be seen the diagram of deflection variations through-in thickness. **Figure 10** shows the deflection variations through-in the thickness for different amounts of temperatures assuming $q_z = 0$.

Figure 9. Deflection changes through-in thickness for different values of temperature under uniform loading $q_z = 1$ GPa

Figure 10. Deflection changes through-in thickness for different values of temperature and neglecting the transverse loading ($q_z = 0$)

Figure 11. The effect of moisture on the three-dimensional results of very thick FGM structure

In this paper, the effect of humid environment on the results of three-dimensional analysis has been attended. It was concluded that if the thermal environment is considered, only the results of three-dimensional analysis can be accepted because the variations of ε_z through the thickness will be significant. **Figure 11** shows the variation of deflection through the thickness for different amounts of $\Box H$. It is observed that with increase of $\Box H$ the deflection variation through the thickness is intensified. The rate of increment for deflection is similar for different values of $\Box H$ as it can be seen for $\Box T$ in **Figure 9** and **10**. Consequently, all obtained behaviors for thermal environment can be concluded for hygro-thermal environment too. Neglecting the strain variations through the thickness (q_z) can result in serious errors when the effect of humidity is considered in the analysis. The deflection varies from 0.0065 to 0.007 ($z = h / 2$) for $\Box H = 0$ and maximum $\Box H = 1$ respectively which is a growth approximately by 8%. The mentioned explanation is about 100% for temperature increment from $\Box T$ = 100 to 1000 in **Figure 9**. Consequently, the temperature plays more important role for the increase of deformation rather than the humidity.

In this paper, in addition to comparing the results of CUFQT and the exact three-dimensional theories, the results of the third-order shear deformation theory (TSDT) are proposed. In recent years, higher-order shear deformation theories have been used widely to give more accurate results (Ebrahimi and Heidari 2019). In continue, the governing equations will be presented based on the TSDT theory. The displacement fields for TSDT plate theory can be found in Dastjerdi and Jabbarzadeh 2016. The TSDT is one of the higher-order theories that is used to study the mechanical behavior of thick plates and provides more accurate results in comparison with the CLPT and FSDT theories (especially for thick plates). **Figure 12 (a, b)** shows the deflection variations along the thickness for the CUFQT and TSDT theories for different temperatures. The thickness of the sheet in this problem is $h = 0.5m$. In all three graphs, it can be seen that the deflection changes through-in thickness for the TSDT theory will be constant. Because TSDT theory neglects the strain variations through the direction of thickness ($\varepsilon_z = 0$). Therefore, a constant amount for deflection will be obtained through the thicknesses (z). The two TSDT and CUFQT charts cut each other at a certain point. In other words, the result of the two theories in this value of z is equal to each other. It is observed that with increasing temperature this value is tended to $z = 0$. But a remarkable point is the distance between the maximum deflection of the CUFQT and the TSDT with increasing ambient temperature. So that this maximum deflection difference for $\Box T$ = 600 C^0 (**Figure 12 (b)**) between the two theories of TSDT and CUFQT is about 300%. Therefore, other results related to the theory of TSDT are not acceptable and the results of CUFQT should be used.

(a) (b)

Figure 12. Comparison between the results of present paper (CUFQT) and TSDT analysis for an annular/circular FGM plate with thickness h = 0.5m (a) $\Box T = 0$ (b) $\Box T$ = 600 C^0

Figure 13 (a) and **(b)** are presented to show the dynamic deflection changes at different values of porosity coefficients. **Figure 13 (a)** is drawn when the porosity is even, and **Figure 13 (b)** is shown when the inner porosity of the disk is uneven. First, by comparing the two cases, it can be

concluded that the deflection will be higher if the porosity is even. The reason may be that the material is softer in this state. On the other hand, the slope of the change in deflections along the thickness is greater in even porosity than uneven one. That is, the difference in deflections in the lower layers of thickness is greater than the upper layers in materials with even distribution of porosity. The cause can be further reducing of deflections in this case. Also, the greater the lambda coefficient, the greater the difference.

(a) (b)

Figure 13. The variations of deflection through the thickness for different values of the structural porosity defect (a) even (b) uneven types

The following **Figure 14** is plotted on the basis of dynamic deflection variations for different rotational velocities. As can be seen, the maximum deflection is not at the center of the thickness, but at the upper surface. The reason can be three-dimensional elasticity analysis that in addition to the vertical deflection after loading, the disc will also have some reductions in thickness, which will naturally be the largest at the highest levels of the thickness. It is interesting to note that as the disk rotation velocity increases, the difference between the results of the different rotational velocities at the upper and lower levels of the thickness is minimal. The cause may be the shear stresses that rotary discs usually face. It is recalled that the shear stress values are usually zero at the upper and lower free surfaces of the sheets and have the highest values near the middle plans of thickness of plates. Hence, as the disk rotation increases, its shear stress is increased and therefore the difference in the static and dynamic cases results in the higher shear stress layers.

In **Figure 15**, due to rotational velocities variations based on *rpm*, the results are presented in several porosities. The output of the results is based on the parameter R_r (%) that is percentage of dynamic to static deflection ($R_r = 100 \times \left(\frac{w_{dynamics}}{w_{statics}} - 1\right)$). $w_{dynamics}$ and $w_{statics}$ represents the deflection of outer radius $r_o(z = +\frac{h}{2})$ in a constant rotating velocity and the static status ($\omega = 0$) respectively. As it turns out, in the lower rotations the amount of porosity in the material does not differ much from the results in the case where the material has no porosity. But with the increase in disk rotational velocity, the importance of examining porosity within the disk will be much greater. This can be understood from the discrepancy between the results of different porosity coefficient values. Clearly, the larger the numerical porosity coefficient, the greater the difference. Interestingly, as the porosity coefficient increases, the dynamic to static deflection results in a higher value, leading to the very valuable conclusion that in high porosity materials the dynamic to static deflection ratio will have large values compared to non-porous material analysis. And so, the dynamic safety factor will go further than the static one. In fact, since many industrial and advanced materials in the manufacturing process may have some porosities, therefore, in the design of high rotational velocity circular discs, dynamic analysis must be performed on the basis of impurities and porosity in the material.

Figure 14. The effect of rotating velocity on the three-dimensional deflection analysis of FGM rotating disk

Figure 15. Variations of parameter R_r due to the increase of rotating velocity (*rpm*) of

disk for different amounts of uneven porosity □(Lambda)

5. Conclusions and remarks

In this study, two highly efficient quasi three-dimensional theories were applied and presented for the analysis of thick and very thick FGM rotating disks in the hygro-thermal environment. The structure was considered to have porosity defect which is a normal task and decreases the strength of structure. The governing equations on the basis of these quasi three-dimensional theories and the assumptions of the nonlinear strain of von Kármán were obtained using the principle of minimum potential energy and were solved by SAPM solving method. The efficiency and accuracy of the presented theories were proved by comparing the results with other available articles and ABAQUS software. The effect of some important parameters affecting the results such as thickness, comparison between the results of applied theories with the exact three-dimensional elasticity theory, loading, hygro-thermal environment and rotating velocity was conducted and further studied. In summary, the important results of this research can be categorized as follows:

1. The results of the theories applied and presented in this article are very similar to the results of the exact three-dimensional elasticity theory.
2. The results of CUFQT and SQT are so close and due to simpler formulations, the use of SQT is recommended in 3D analysis.
3. Third and fifth-order models of CUFQT give so similar results and the differences are inconsiderable in comparison with the advantages of third-order CUFQT. However, the fifth-order theory gives the more accurate results especially for very thick structures.
4. The rate of convergence of the results from the CUFQT is more than the exact three-dimensional elasticity theory. Also, the time that the results are obtained using the CUFQT is much shorter than the exact 3D theory.
5. By using the exact 3D theory, the governing equations for the axisymmetric sector sheet is a set of third-order partial differential equations. But for this case, a set of second-order partial differential equations will be extracted in the CUFQT, which is much easier to solve.
6. In general, the use of CUFQT reduces the order of obtained governing partial differential equations. While the strain variations through the thickness (similar to the exact 3D elasticity theory) are maintained ($\varepsilon_z \neq 0$).
7. The results of the applied and presented theories will be much more accurate rather than the results of the plate theories such as CLPT, FSDT, TSDT and HSDT.
8. Using the applied and presented theories when the structure is embedded in a hygro-thermal environment gives more reliable results. However, the temperature has more effects on the results in comparison with the humidity. While the other plate theories (even higher-order theories such as TSDT) give unacceptable results, especially for moderately thick and thick plates.
9. The greater the thickness of the sheet, the results of three-dimensional analysis will be more accurate.
10. The porosity decreases the strength of FGM rotating disk. Even type of porosity reduces the strength of structure more than uneven one.
11. The rotating velocity of FGM disk causes the increment in deformation. However, the effect of rotating velocity is ascending due to the increase of ω. In other words, whatever the rotating velocity increases, the three-dimensional deflection grows ascendingly.

12. The two quasi three-dimensional theories in this paper, eliminates the disadvantages of the exact 3D theory such as the higher-order partial differential equations which can be seen in completely axisymmetric 3D problems.

References

Abualnour, M., M. S. A. Houari, A. Tounsi, E. A. Adda Bedia, and S. R. Mahmoud. 2018. A novel quasi-3D trigonometric plate theory for free vibration analysis of advanced composite plates. *Composite Structures* 184:688–697.

Adhikari, B., and B. N. Singh .2018. An efficient higher order non-polynomial Quasi 3-D theory for dynamic responses of laminated composite plates. *Composite Structures* 189:386–397.

Alibeigloo, A. 2011. Free vibration analysis of nano-plate using three-dimensional theory of elasticity. *Acta Mechanica* 222:149–159.

Benahmed, A., M. S. A. Houari, S. Benyoucef, and A. Tounsi. 2017. A novel quasi-3D hyperbolic shear deformation theory for functionally graded thick rectangular plates on elastic foundation. *Geomechanics and Engineering* 12:9–34.

Bessaim, A., M. S. A. Houari, F. Bernard, and A. Tounsi. 2015. A nonlocal quasi-3D trigonometric plate model for free vibration behaviour of micro/nanoscale plates. *Structural Engineering and Mechanics* 56:223–240.

Bouafia, K. h., A. Kaci, M. S. A. Houari, A. Benzair, and A. Tounsi. 2017. A nonlocal quasi-3D theory for bending and free flexural vibration behaviors of functionally graded nanobeams. *Smart Structures and Systems* 19:115–126.

Carrera, E., S. Brischetto, M. Cinefra, and M. Soave. 2011. Effects of thickness stretching in functionally graded plates and shells. *Composites Part B: Engineering* 42:123–133.

Chaubey, A. K., A. Kumar, and A. Chakrabarti. 2018. Novel shear deformation model for moderately thick and deep laminated composite conoidal shell. *Mechanics Based Design of Structures and Machines, An International Journal* 46 (5):650–668.

Dastjerdi, S., and B. Akgöz. 2018. New static and dynamic analyses of macro and nano FGM plates using exact three-dimensional elasticity in thermal environment. *Composite Structures* 192:626–641.

Dastjerdi, S., and B. Akgöz. 2019. On the statics of fullerene structures. *International Journal of Engineering Science* 142:125-144.

Dastjerdi, S., B. Akgöz, and L. Yazdanparast. 2018. A new approach for bending analysis of bilayer conical graphene panels considering nonlinear van der Waals force. *Composites Part B: Engineering* 150:124–134.

Dastjerdi, S., B. Akgöz, and Ö. Civalek. 2020. On the effect of viscoelasticity on behavior of gyroscopes. *International Journal of Engineering Science* 149:103236.

Dastjerdi, S., and M. Jabbarzadeh. 2016. Non-Local Thermo-Elastic Buckling Analysis of Multi-Layer Annular/Circular Nano-Plates Based on First and Third Order Shear Deformation Theories Using DQ Method. *Journal of solid Mechanics* 8:859–874.

Dastjerdi, S., and Y. Tadi Beni. 2019. A novel approach for nonlinear bending response of macro-and nanoplates with irregular variable thickness under nonuniform loading in thermal environment. *Mechanics Based Design of Structures and Machines, An International Journal* 47:453–478.

Ebrahimi, F., and E. Heidari. 2019. Surface effects on nonlinear vibration of embedded functionally graded nanoplates via higher order shear deformation plate theory. *Mechanics Based Design of Structures and Machines, An International Journal* 26:671–699.

Farzam-Rad, S. A., B. Hassani, and A. Karamodin. 2017. Isogeometric analysis of functionally graded plates using a new quasi-3D shear deformation theory based on physical neutral surface. *Composites Part B: Engineering* 108:174–189.

Jena, S. K., Chakraverty, S., Malikan, M., F. Tornabene. 2020. Effects of surface energy and surface residual stresses on vibro-thermal analysis of chiral, zigzag, and armchair types of SWCNTs using refined beam theory. *Mechanics Based Design of Structures and Machines, An International Journal*. https://doi.org/10.1080/15397734.2020.1754239

Jin, G., Z. h., Su, T. Ye, and S. Gao. 2015. Three-dimensional free vibration analysis of functionally graded annular sector plates with general boundary conditions. *Composites Part B: Engineering* 83:352–366.

Karami, B., M. Janghorban, and L. Li. 2018. On guided wave propagation in fully clamped porous functionally graded nanoplates. *Acta Astronautica* 143:380-390.

Karami, B., M. Janghorban, and T. Rabczuk. 2019a. Analysis of elastic bulk waves in functionally graded triclinic nanoplates using a quasi-3D bi-Helmholtz nonlocal strain gradient model. *European Journal of Mechanics - A/Solids* 78:103822.

Karami, B., M. Janghorban, and T. Rabczuk. 2019b. Static analysis of functionally graded anisotropic nanoplates using nonlocal strain gradient theory. *Composite Structures* 227:111249.

Karami, B., M. Janghorban, D. Shahsavari, and A. Tounsi. 2018. A size-dependent quasi-3D model for wave dispersion analysis of FG nanoplates. *Steel and Composite Structures* 28:99-110.

Karami, B., M. Janghorban, and A. Tounsi. 2019. Wave propagation of functionally graded anisotropic nanoplates resting on Winkler-Pasternak foundation. *Structural Engineering and Mechanics* 70:55-66.

Karami, B., D. Shahsavari, M. Janghorban, and L. Li. 2019. On the resonance of functionally graded nanoplates using bi-Helmholtz nonlocal strain gradient theory. *International Journal of Engineering Science* 144:103143.

Li, C. 2017. Nonlocal thermo-electro-mechanical coupling vibrations of axially moving piezoelectric nanobeams. *Mechanics Based Design of Structures and Machines, An International Journal* 45 (4):463–478.

Liu, Sh., T. Yu, T. Q. Bui, Sh. Yin, D. K. Thai, and S. Tanaka. 2017. Analysis of functionally graded plates by a simple locking-free quasi-3D hyperbolic plate isogeometric method. *Composites Part B: Engineering* 120:182–196.

Mahmoudi, A., S. Benyoucef, A. Tounsi, A. Benachour, E. A. Adda Bedia, and S. R. Mahmoud. 2017. A refined quasi-3D shear deformation theory for thermo-mechanical behavior of functionally graded sandwich plates on elastic foundations. *Journal of Sandwich Structures & Materials* 1–24.

Matsunaga, H. 2004. A comparison between 2-D single-layer and 3-D layerwise theories for computing interlaminar stresses of laminated composite and sandwich plates subjected to thermal loadings. *Composite Structures* 64:161-177.

Matsunaga, H. 2008a. Free vibration and stability of functionally graded shallow shells according to a 2D higher-order deformation theory. *Composite Structures* 84:132-146.

Matsunaga, H. 2008b. Free vibration and stability of functionally graded circular cylindrical shells according to a 2D higher-order deformation theory. *Composite Structures* 84:132-146.

Matsunaga, H. 2009. Thermal buckling of functionally graded plates according to a 2D higher-order deformation theory. *Composite Structures* 90:76-86.

Malikan, M. 2017. Electro-mechanical shear buckling of piezoelectric nanoplate using modified couple stress theory based on simplified first order shear deformation theory. *Applied Mathematical Modeling* 48:196-207.

Malikan, M., and V. A. Eremeyev. 2020. A new hyperbolic-polynomial higher-order elasticity theory for mechanics of thick FGM beams with imperfection in the material composition. *Composite Structures* 249:112486.

Malikan, M., M. Jabbarzadeh, and S. Dastjerdi. 2017. Non-linear Static stability of bi-layer carbon nanosheets resting on an elastic matrix under various types of in-plane shearing loads in thermo-elasticity using nonlocal continuum. *Microsystem Technologies* 23:2973-2991.

Malikan, M., and V. B. Nguyen. 2018. Buckling analysis of piezo-magnetoelectric nanoplates in hygrothermal environment based on a novel one variable plate theory combining with higher-order nonlocal strain gradient theory. *Physica E: Low-dimensional Systems and Nanostructures* 102:8-28.

Malikan, M., F. Tornabene, and R. Dimitri. 2018. Nonlocal three-dimensional theory of elasticity for buckling behavior of functionally graded porous nanoplates using volume integrals. *Materials Research Express* 5:095006.

Mantari, J. L., and C. G. Soares. 2012. Generalized hybrid quasi-3D shear deformation theory for the static analysis of advanced composite plates. *Composite Structures* 94:2561–2575.

Mantari, J. L., and C. G. Soares. 2014. Four-unknown quasi-3D shear deformation theory for advanced composite plates. *Composite Structures* 109:231–239.

Mantari, J. L., and E. V. Granados. 2015. Thermoelastic behavior of advanced composite sandwich plates by using a new 6 unknown quasi-3D hybrid type HSDT. *Composite Structures* 126:132–144.

Neves, A. M. A., A. J. M. Ferreira, E. Carrera, C. M. C. Roque, M. Cinefra, R. M. N. Jorgea, and C. M. M. Soares. 2012a. A quasi-3D sinusoidal shear deformation theory for the static and free vibration analysis of functionally graded plates. *Composites Part B: Engineering* 43:711–725.

Neves, A. M. A., A. J. M. Ferreira, E. Carrera, M., Cinefra, C. M. C. Roque, R. M. N. Jorge, and C. M. M. Soares. 2012b. A quasi-3D hyperbolic shear deformation theory for the static and free vibration analysis of functionally graded plates. *Composite Structures* 94:1814–1825.

Neves, A. M. A., A. J. M. Ferreira, E. Carrera, M. Cinefra, C. M. C. Roque, R. M. N. Jorge, and C. M. M. Soares. 2013. Static, free vibration and buckling analysis of isotropic and sandwich functionally graded plates using a quasi-3D higher-order shear deformation theory and a meshless technique. *Composites Part B: Engineering* 44:657–674.

Nguyen, H. X., T. N. Nguyen, M. Abdel-Wahab, S. P. A. Bordas, H. Nguyen-Xuan, and T. P. Vo. 2017. A Refined Quasi-3D Isogeometric Analysis for Functionally Graded Microplates based on the Modified Couple Stress Theory. *Computer Methods in Applied Mechanics and Engineering* 313:904–940.

Nikbakht, S., S. Jedari Salami, and M. Shakeri. 2017. Three dimensional analysis of functionally graded plates up to yielding, using full layer-wise finite element method. *Composite Structures* 182:99–115.

Patil, Y. T., T. Kant, and Y. M. Desai. 2018. Comparison of Three Dimensional Elasticity Solutions for Functionally Graded Plates. *Composite Structures* 202:424–435.

Shahsavari, D., M. Shahsavari, L. Li, and B. Karami. 2018. A novel quasi-3D hyperbolic theory for free vibration of FG plates with porosities resting on Winkler/Pasternak/Kerr foundation. *Aerospace Science and Technology* 72:134-149.

Thai, H. T., and S. E. Kim. 2013. A simple quasi-3D sinusoidal shear deformation theory for functionally graded plates. *Composite Structures* 99:172–180.

Thai, H. T., T. P. Vo, T. Q. Bui, and T. K. Nguyen. 2014. A quasi-3D hyperbolic shear deformation theory for functionally graded plates. *Acta Mechanica* 225:951–964.

Wu, C. P., K. H. Chiu, and Y. M. Wang. 2011. RMVT-based meshless collocation and element-free Galerkin methods for the quasi-3D analysis of multilayered composite and FGM plates. *Composite Structures* 93:923–943.

Zenkour, A. M. 2018. A quasi-3D refined theory for functionally graded single-layered and sandwich plates with porosities. *Composite Structures* 201:38–48.

Appendix.

A.1. The quasi governing equations:

$$\delta u_1 : \frac{dN_r}{dr} + \frac{1}{r}\left(N_r - N_\theta\right) + \rho_1 r\omega^2 = 0 \tag{1}$$

$$\delta u_2 : \frac{dM_r}{dr} + \frac{1}{r}\left(M_r - M_\theta\right) - Q_{rz} = 0 \tag{2}$$

$$\delta u_3 : \frac{dP_r}{dr} + \frac{1}{r}\left(P_r - P_\theta\right) - 2M_{rz} = 0 \tag{3}$$

$$\delta u_4 : \frac{dH_r}{dr} + \frac{1}{r}\left(H_r - H_\theta\right) - 3P_{rz} = 0 \tag{4}$$

$$\delta u_5 : \frac{dY_r}{dr} + \frac{1}{r}\left(Y_r - Y_\theta\right) - 4H_{rz} = 0 \tag{5}$$

$$\delta u_6 : \frac{dS_r}{dr} + \frac{1}{r}\left(S_r - S_\theta\right) - 5Y_{rz} = 0 \tag{6}$$

$$\delta w_1 : \frac{dQ_{rz}}{dr} + \frac{1}{r}Q_{rz} + q_z + k_w\left(w_1 + w_2\left(\frac{h}{2}\right) + w_3\left(\frac{h}{2}\right)^2 + w_4\left(\frac{h}{2}\right)^3 + w_5\left(\frac{h}{2}\right)^4 + w_6\left(\frac{h}{2}\right)^5\right) +$$
$$k_p\left(\nabla^2 w_1 + \nabla^2 w_2\left(\frac{h}{2}\right) + \nabla^2 w_3\left(\frac{h}{2}\right)^2 + \nabla^2 w_4\left(\frac{h}{2}\right)^3 + \nabla^2 w_5\left(\frac{h}{2}\right)^4 + \nabla^2 w_6\left(\frac{h}{2}\right)^5\right) + \tag{7}$$
$$\frac{N_\theta}{r}\frac{dw_1}{dr} + N_r\left(\frac{d^2 w_1}{dr^2}\right) = 0$$

$$\delta w_2 : \frac{dM_{rz}}{dr} + \frac{1}{r}M_{rz} - N_z + q_z\left(\frac{h}{2}\right) + k_w\left(w_1\left(\frac{h}{2}\right) + w_2\left(\frac{h}{2}\right)^2 + w_3\left(\frac{h}{2}\right)^3 + w_4\left(\frac{h}{2}\right)^4 +\right.$$
$$\left. w_5\left(\frac{h}{2}\right)^5 + w_6\left(\frac{h}{2}\right)^6\right) + k_p\left(\nabla^2 w_1\left(\frac{h}{2}\right) + \nabla^2 w_2\left(\frac{h}{2}\right)^2 + \nabla^2 w_3\left(\frac{h}{2}\right)^3 + \nabla^2 w_4\left(\frac{h}{2}\right)^4 + \right. \tag{8}$$
$$\left.\nabla^2 w_5\left(\frac{h}{2}\right)^5 + \nabla^2 w_6\left(\frac{h}{2}\right)^6\right) + \left(\frac{M_\theta}{r} + Q_{rz}\right)\frac{dw_2}{dr} + M_r\left(\frac{d^2 w_2}{dr^2}\right) = 0$$

$$\delta w_3 : \frac{dP_{rz}}{dr} + \frac{1}{r}P_{rz} - 2M_z + q_z\left(\frac{h}{2}\right)^2 + k_w\left(w_1\left(\frac{h}{2}\right)^2 + w_2\left(\frac{h}{2}\right)^3 + w_3\left(\frac{h}{2}\right)^4 + w_4\left(\frac{h}{2}\right)^5 + w_5\left(\frac{h}{2}\right)^6 + w_6\left(\frac{h}{2}\right)^7\right) + k_p\left(\nabla^2 w_1\left(\frac{h}{2}\right)^2 + \nabla^2 w_2\left(\frac{h}{2}\right)^3 + \nabla^2 w_3\left(\frac{h}{2}\right)^4 + \nabla^2 w_4\left(\frac{h}{2}\right)^5 + \nabla^2 w_5\left(\frac{h}{2}\right)^6 + \nabla^2 w_6\left(\frac{h}{2}\right)^7\right) + \left(\frac{P_\theta}{r} + 2M_{rz}\right)\frac{dw_3}{dr} + P_r\left(\frac{d^2 w_3}{dr^2}\right) = 0 \quad (9)$$

$$\delta w_4 : \frac{dH_{rz}}{dr} + \frac{1}{r}H_{rz} - 3P_z + q_z\left(\frac{h}{2}\right)^3 + k_w\left(w_1\left(\frac{h}{2}\right)^3 + w_2\left(\frac{h}{2}\right)^4 + w_3\left(\frac{h}{2}\right)^5 + w_4\left(\frac{h}{2}\right)^6 + w_5\left(\frac{h}{2}\right)^7 + w_6\left(\frac{h}{2}\right)^8\right) + k_p\left(\nabla^2 w_1\left(\frac{h}{2}\right)^3 + \nabla^2 w_2\left(\frac{h}{2}\right)^4 + \nabla^2 w_3\left(\frac{h}{2}\right)^5 + \nabla^2 w_4\left(\frac{h}{2}\right)^6 + \nabla^2 w_5\left(\frac{h}{2}\right)^7 + \nabla^2 w_6\left(\frac{h}{2}\right)^8\right) + \left(\frac{H_\theta}{r} + 3P_{rz}\right)\frac{dw_4}{dr} + H_r\left(\frac{d^2 w_4}{dr^2}\right) = 0 \quad (10)$$

$$\delta w_5 : \frac{dY_{rz}}{dr} + \frac{1}{r}Y_{rz} - 4H_z + q_z\left(\frac{h}{2}\right)^4 + k_w\left(w_1\left(\frac{h}{2}\right)^4 + w_2\left(\frac{h}{2}\right)^5 + w_3\left(\frac{h}{2}\right)^6 + w_4\left(\frac{h}{2}\right)^7 + w_5\left(\frac{h}{2}\right)^8 + w_6\left(\frac{h}{2}\right)^9\right) + k_p\left(\nabla^2 w_1\left(\frac{h}{2}\right)^4 + \nabla^2 w_2\left(\frac{h}{2}\right)^5 + \nabla^2 w_3\left(\frac{h}{2}\right)^6 + \nabla^2 w_4\left(\frac{h}{2}\right)^7 + \nabla^2 w_5\left(\frac{h}{2}\right)^8 + \nabla^2 w_6\left(\frac{h}{2}\right)^9\right) + \left(\frac{Y_\theta}{r} + 4H_{rz}\right)\frac{dw_5}{dr} + Y_r\left(\frac{d^2 w_5}{dr^2}\right) = 0 \quad (11)$$

$$\delta w_6 : \frac{dS_{rz}}{dr} + \frac{1}{r}S_{rz} - 5Y_z + q_z\left(\frac{h}{2}\right)^5 + k_w\left(w_1\left(\frac{h}{2}\right)^5 + w_2\left(\frac{h}{2}\right)^6 + w_3\left(\frac{h}{2}\right)^7 + w_4\left(\frac{h}{2}\right)^8 + w_5\left(\frac{h}{2}\right)^9 + w_6\left(\frac{h}{2}\right)^{10}\right) + k_p\left(\nabla^2 w_1\left(\frac{h}{2}\right)^5 + \nabla^2 w_2\left(\frac{h}{2}\right)^6 + \nabla^2 w_3\left(\frac{h}{2}\right)^7 + \nabla^2 w_4\left(\frac{h}{2}\right)^8 + \nabla^2 w_5\left(\frac{h}{2}\right)^9 + \nabla^2 w_6\left(\frac{h}{2}\right)^{10}\right) + \left(\frac{S_\theta}{r} + 5Y_{rz}\right)\frac{dw_6}{dr} + S_r\left(\frac{d^2 w_6}{dr^2}\right) = 0 \quad (12)$$

The stress resultants in the above relations are expressed below ($\rho(r)$ is the density of the structure along the radius (r) direction.):

$$(N_r, N_\theta, N_z, Q_{rz}) = \int_{-\frac{h}{2}}^{\frac{h}{2}} (\sigma_r, \sigma_\theta, \sigma_z, \sigma_{rz})\, dz \quad (13)$$

$$(M_r, M_\theta, M_z, M_{rz}) = \int_{-\frac{h}{2}}^{\frac{h}{2}} (\sigma_r, \sigma_\theta, \sigma_z, \sigma_{rz})\, z\, dz \quad (14)$$

$$(P_r, P_\theta, P_z, P_{rz}) = \int_{-\frac{h}{2}}^{\frac{h}{2}} (\sigma_r, \sigma_\theta, \sigma_z, \sigma_{rz})\, z^2\, dz \quad (15)$$

$$(H_r, H_\theta, H_z, H_{rz}) = \int_{-\frac{h}{2}}^{\frac{h}{2}} (\sigma_r, \sigma_\theta, \sigma_z, \sigma_{rz})\, z^3\, dz \quad (16)$$

$$(Y_r, Y_\theta, Y_z, Y_{rz}) = \int_{-\frac{h}{2}}^{\frac{h}{2}} (\sigma_r, \sigma_\theta, \sigma_z, \sigma_{rz})\, z^4\, dz \quad (17)$$

$$\left(S_r, S_\theta, S_z, S_{rz}\right) = \int_{-\frac{h}{2}}^{\frac{h}{2}} \left(\sigma_r, \sigma_\theta, \sigma_z, \sigma_{rz}\right) z^5 dz \tag{18}$$

$$\rho_1 = \int_{-\frac{h}{2}}^{\frac{h}{2}} \rho(r) dz \tag{19}$$

A.2. The governing equations based on the simplified quasi three-dimensional theory (SQT):

$$\delta u_1 : \frac{dN_r}{dr} + \frac{1}{r}\left(N_r - N_\theta\right) + \rho_1 r\omega^2 = 0 \tag{1}$$

$$\delta u_2 : \frac{dP_r}{dr} + \frac{1}{r}\left(P_r - P_\theta\right) - P_{rz} = 0 \tag{2}$$

$$\delta w_1 : \frac{dN_{rz}}{dr} + \frac{1}{r}N_{rz} + q_z = 0 \tag{3}$$

$$\delta w_2 : \frac{dH_{rz}}{dr} + \frac{1}{r}H_{rz} - N_z + q_z\left(\left(g(z)\right)\Big|_{z=\frac{h}{2}}\right) = 0 \tag{4}$$

The stress resultants in above equations are expressed below:

$$\left(N_r, N_\theta, N_{rz}\right) = \int_{-\frac{h}{2}}^{\frac{h}{2}} \left(\sigma_r, \sigma_\theta, \sigma_{rz}\right) dz \tag{5}$$

$$\left(P_r, P_\theta\right) = \int_{-\frac{h}{2}}^{\frac{h}{2}} f(z)\left(\sigma_r, \sigma_\theta\right) dz \tag{6}$$

$$N_z, H_{rz}, P_{rz} = \int_{-\frac{h}{2}}^{\frac{h}{2}} \left[\frac{d}{dz}\left(g(z)\right)\sigma_z, g(z)\sigma_{rz}, \frac{d}{dz}\left(f(z)\right)\sigma_{rz}\right] dz \tag{7-10}$$

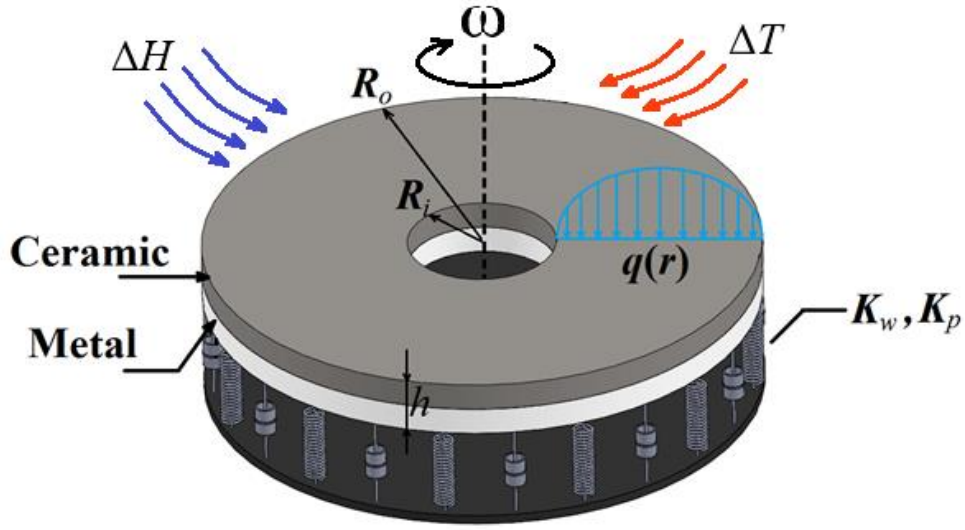

Figure 1. Symmetric annular/circular FGM rotating disk embedded in Winkler-Pasternak elastic foundation under transverse loading q (r)

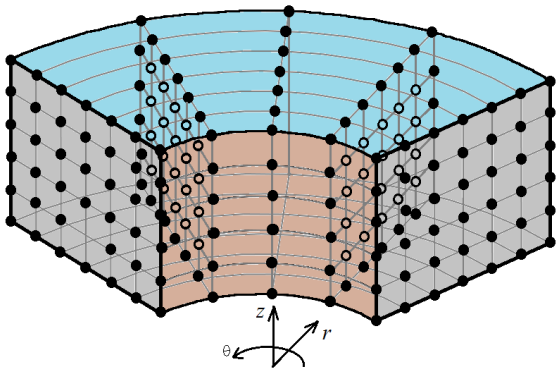

Figure 2. Three-dimensional schematic view of a sector FGM plate in r, θ and z directions

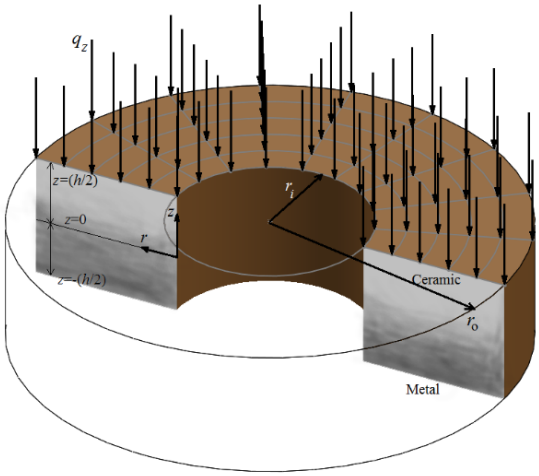

Figure 3. An annular/circular FGM plate under uniform loading (q_z)

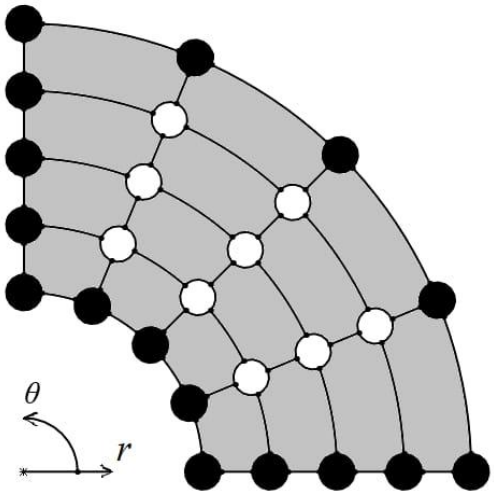

Figure 4. Sample grid points for a sector

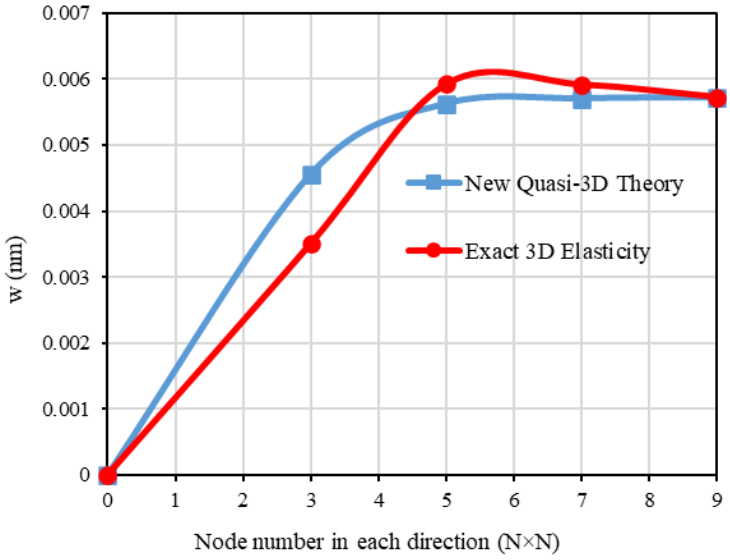

Figure 5. The rate of convergence for the results of CUFQT and the exact three-dimensional elasticity theory

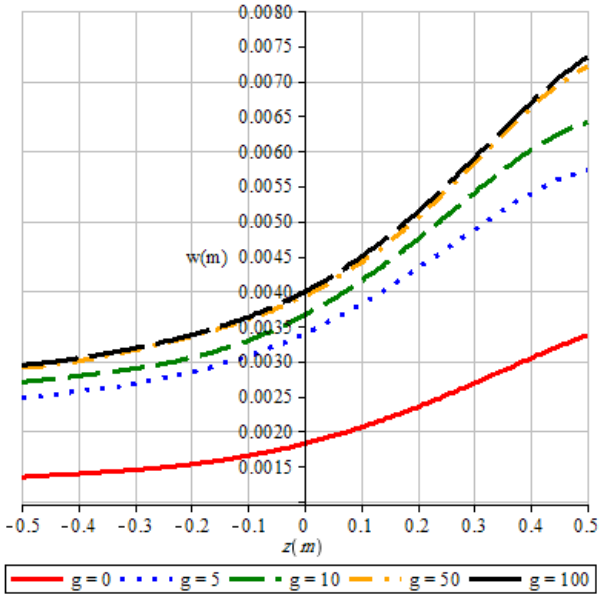

Figure 6. The deflection along the thickness for different values of FGM parameter *g*

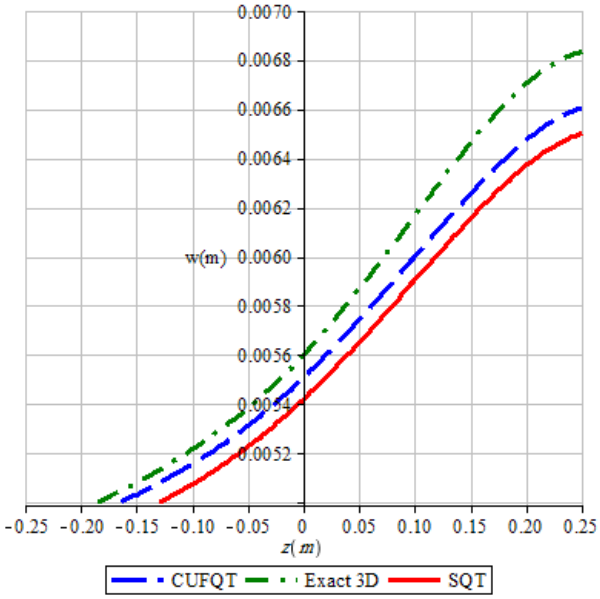

(a)

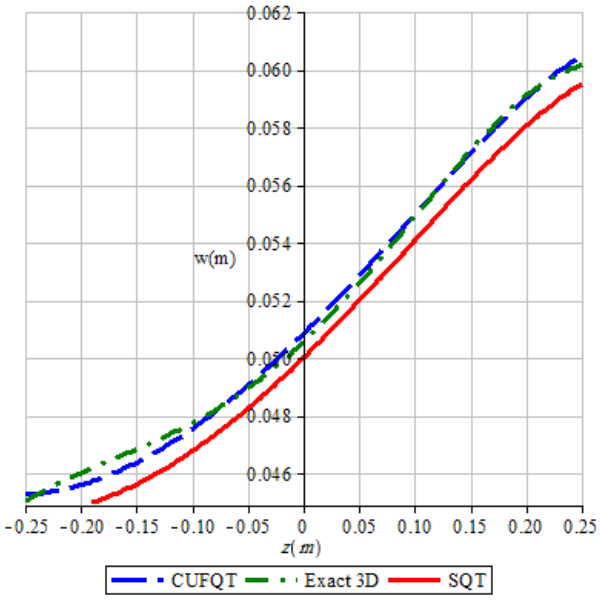

(b)

Figure 7. The results of CUFQT, SQT and the exact 3D theories for different values of loading (a) $q_z = 1$ GPa and (b) $q_z = 10$ GPa

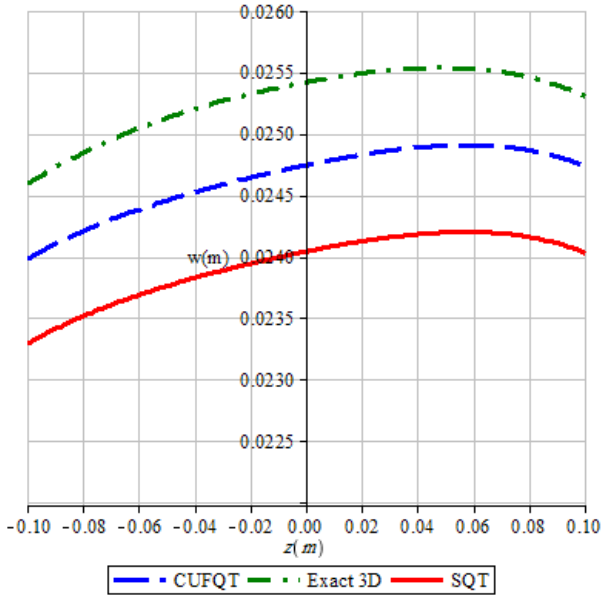

(a)

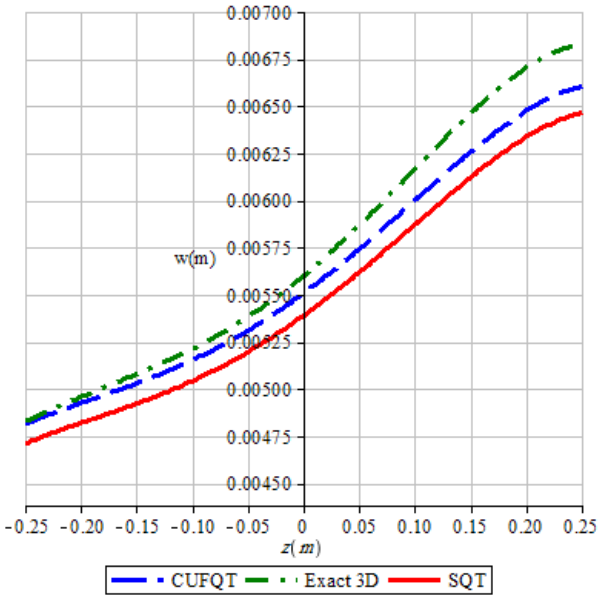

(b)

Figure 8. Comparison between the results of CUFQT, SQT and exact 3D theories for different values of thickness (a) h = 0.2m (b) h = 0.5m

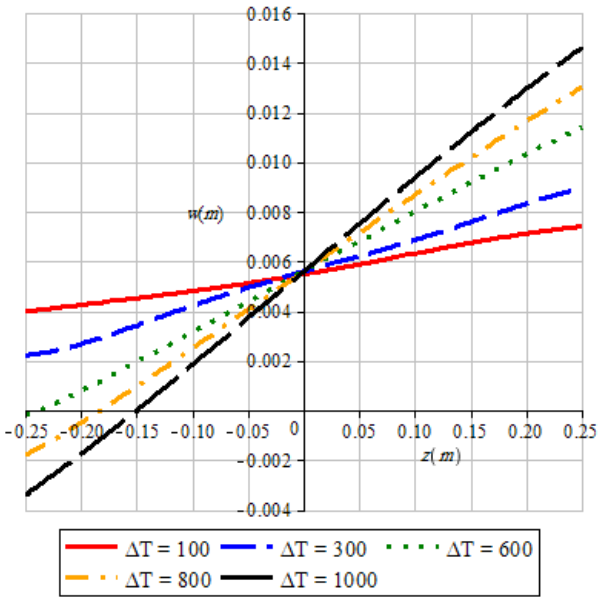

Figure 9. Deflection changes through-in thickness for different values of temperature under uniform loading $q_z = 1$ GPa

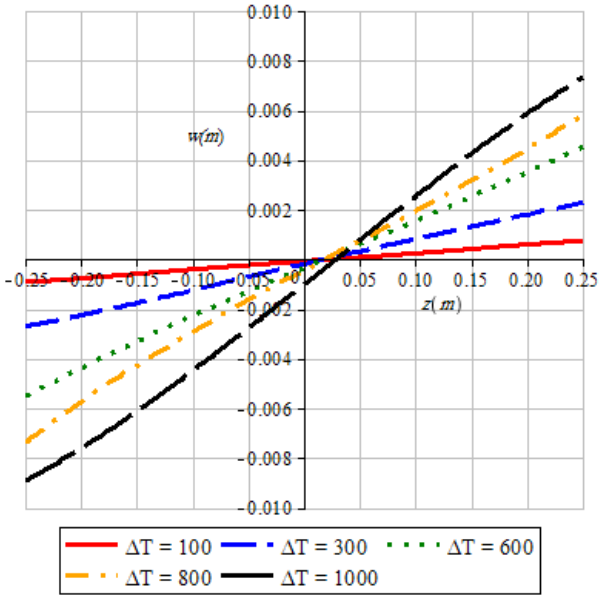

Figure 10. Deflection changes through-in thickness for different values of temperature and neglecting the transverse loading ($q_z = 0$)

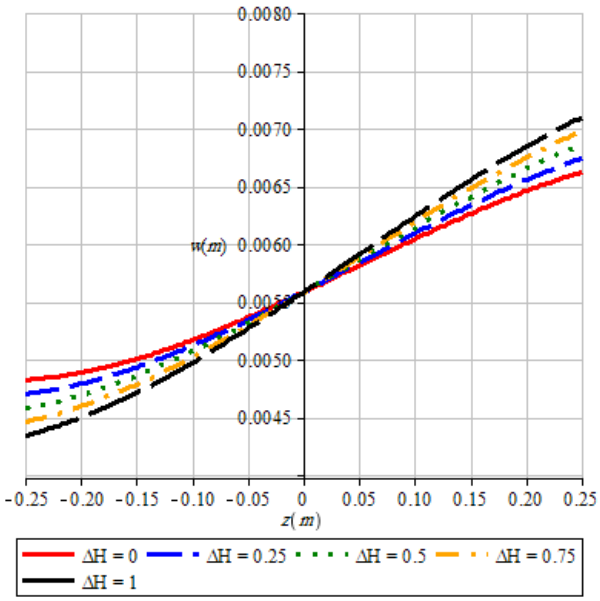

Figure 11. The effect of moisture on the three-dimensional results of very thick FGM structure

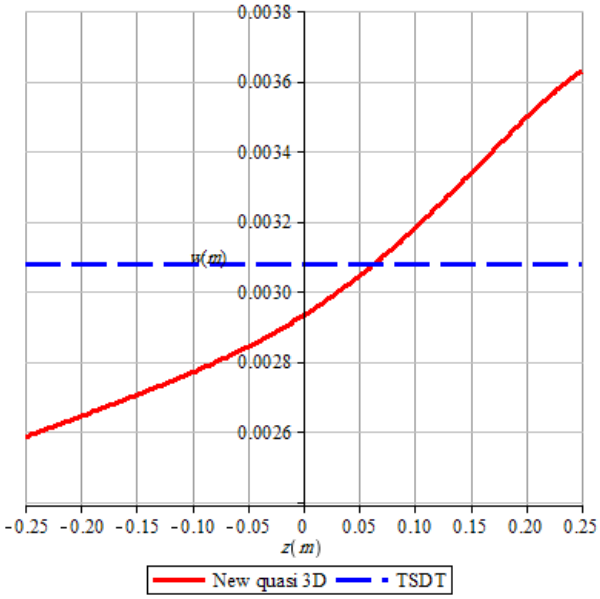

(a)

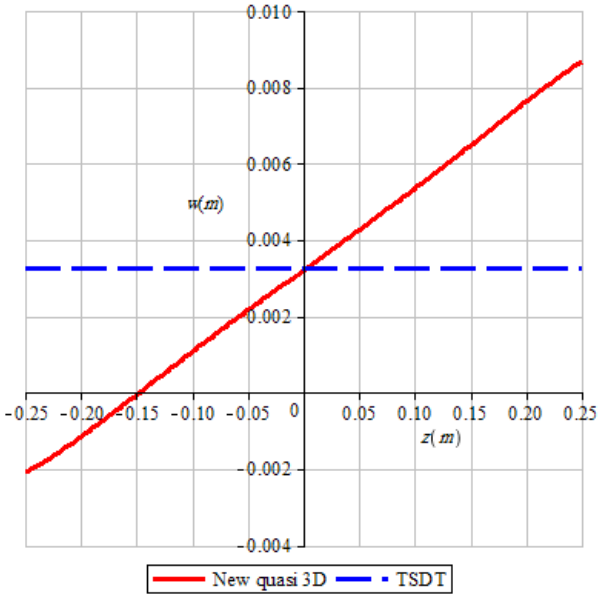

(b)

Figure 12. Comparison between the results of present paper (CUFQT) and TSDT analysis for an annular/circular FGM plate with thickness h = 0.5m (a) $\square T = 0$ (b) $\square T = 600\ C^0$

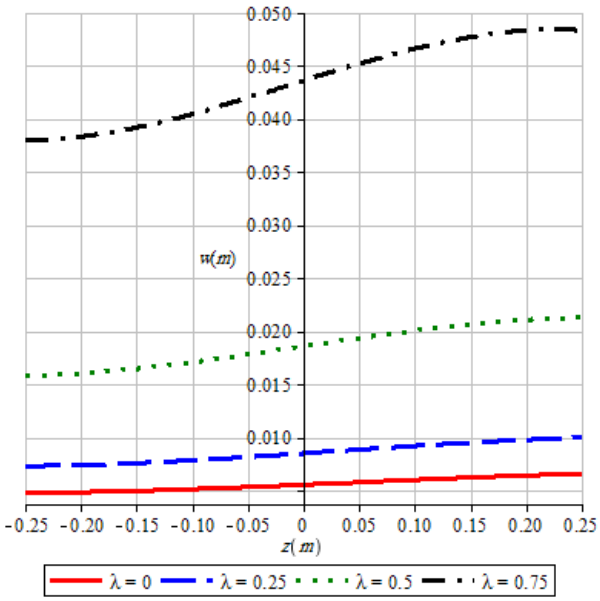

(a)

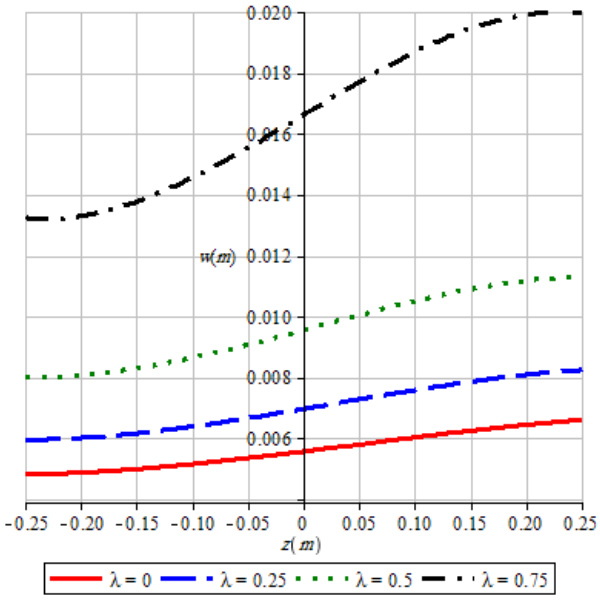

(b)

Figure 13. The variations of deflection through the thickness for different values of the structural porosity defect (a) even (b) uneven types

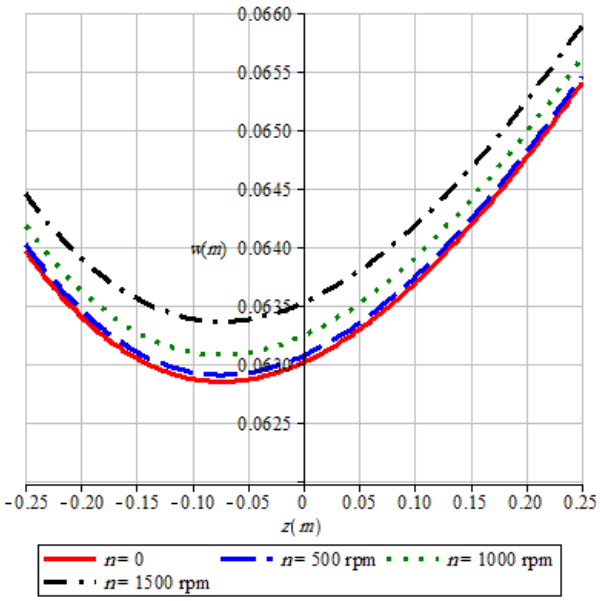

Figure 14. The effect of rotating velocity on the three-dimensional deflection analysis of FGM rotating disk

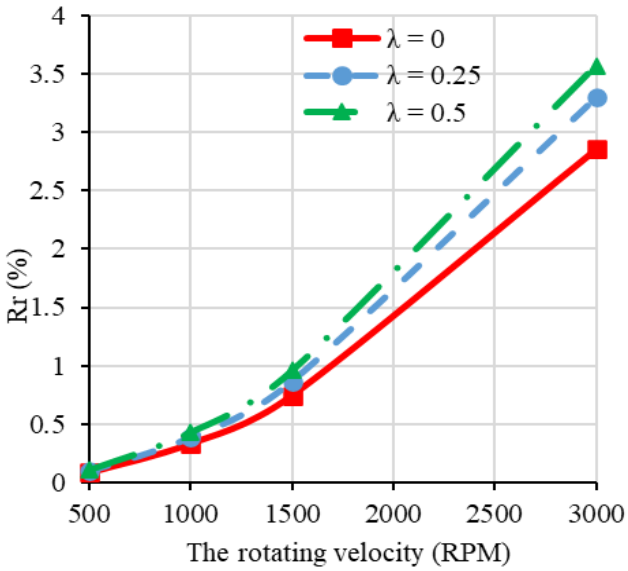

Figure 15. Variations of parameter R_r due to the increase of rotating velocity (*rpm*) of disk for different amounts of uneven porosity □(Lambda)

Table 1. The results of the third and fifth-order CUFQT for different values of thickness and load

		w (h/2) m		
	h (m)	Third-order	Fifth-order	R_{TF}
$q_z = 1\ GPa$	0.1	0.08230	0.08234	0.9995
	0.2	0.02513	0.02512	1.0004
	0.5	0.00662	0.00668	0.9918
	1	0.00405	0.00421	0.9606
$q_z = 2\ GPa$	0.1	0.12080	0.12032	1.0041
	0.2	0.04717	0.04719	0.9996
	0.5	0.01314	0.01323	0.9932
	1	0.00807	0.00838	0.9632

Table 2. Comparison between the CUFQT results of present paper (P.P) and the exact three-dimensional results in (Dastjerdi, and Akgöz 2018)

	Thickness-to-radius ratio, h/a									
	0		0.05		0.1		0.15		0.2	
g	P.P	(Dastjerdi, and Akgöz 2018)	P.P	(Dastjerdi, and Akgöz 2018)	P.P	(Dastjerdi, and Akgöz 2018)	P.P	(Dastjerdi, and Akgöz 2018)	P.P	(Dastjerdi, and Akgöz 2018)
0	2.345	2.521	2.399	2.516	2.487	2.579	2.623	2.701	2.814	2.875
2	1.289	1.386	1.317	1.381	1.361	1.411	1.429	1.471	1.524	1.557
4	1.178	1.267	1.205	1.263	1.244	1.290	1.305	1.344	1.392	1.422
6	1.122	1.206	1.146	1.202	1.184	1.228	1.243	1.280	1.326	1.355
8	1.085	1.167	1.109	1.163	1.147	1.189	1.205	1.241	1.286	1.314
10	1.061	1.141	1.085	1.138	1.121	1.163	1.179	1.214	1.259	1.286
15	1.024	1.101	1.046	1.097	1.083	1.123	1.139	1.173	1.217	1.244
20	1.003	1.078	1.026	1.076	1.061	1.100	1.112	1.145	1.195	1.221
25	0.990	1.064	1.012	1.061	1.048	1.087	1.102	1.135	1.180	1.206
30	0.981	1.055	1.002	1.051	1.038	1.076	1.093	1.125	1.170	1.196
35	0.974	1.047	0.996	1.044	1.031	1.069	1.086	1.118	1.163	1.188
40	0.969	1.042	0.990	1.038	1.025	1.063	1.080	1.112	1.157	1.182
50	0.961	1.033	0.982	1.030	1.017	1.055	1.072	1.104	1.149	1.174
10^2	0.946	1.017	0.967	1.014	1.002	1.039	1.056	1.087	1.132	1.157
10^3	0.931	1.001	0.952	0.998	0.986	1.023	1.040	1.071	1.117	1.141
10^4	0.930	1.000	0.950	0.996	0.985	1.021	1.038	1.069	1.115	1.139
10^5	0.930	1.000	0.950	0.996	0.985	1.021	1.038	1.069	1.115	1.139

Table 3. Validation of the results of present paper (CUFQT) with ABAQUS and TSDT analysis for different values of thickness and boundary conditions

		w (mm)				
	h (m)	ABAQUS	P.P	TSDT	R_{AP}%	R_{TP}%
FC	0.25	72.64	67.46	71.77	-7.1	-6
	0.5	14.76	14.23	14.21	-3.6	+0.1
	1	5.83	5.68	4.17	-2.6	+36.1
CC	0.25	9.60	9.19	9.26	-4.4	-0.8
	0.5	3.77	3.66	3.08	-2.9	+18.9
	1	2.65	2.60	1.29	-1.8	+101.9

Table 4. Runtime for present paper (CUFQT) and the exact three-dimensional elasticity theory for different types of boundary conditions and node numbers

		t (Second)		
	N (Number of nodes)	Exact three-dimensional theory	P.P	R_{PE}(Second)
CC	3	4.40	8.79	-4.39
	5	5.20	10.68	-5.48
	7	16.63	15.05	+1.58
	9	82.45	23.58	+58.87
SS	3	4.20	8.68	-4.48
	5	5.13	10.80	-5.67
	7	17.02	15.45	+1.57
	9	84.18	24.08	+60.10